A Stochastic Tractography System and Applications

by

Tri M. Ngo

Submitted to the Department of Electrical Engineering and Computer Science
in partial fulfillment of the requirements for the degree of

Master of Engineering in Electrical Engineering and Computer Science

at the

MASSACHUSETTS INSTITUTE OF TECHNOLOGY

May 2007
[June 2007]

Author .....
Department of Electrical Engineering and Computer Science
May 28, 2007

Certified by .....
Polina Golland
Assistant Professor
Thesis Supervisor

Certified by .....
Carl-Fredrik Westin
Associate Professor
Thesis Supervisor

Accepted by .....
Arthur C. Smith
Professor of Electrical Engineering
Chairman, Department Committee on Graduate Students

A Stochastic Tractography System and Applications

by

Tri M. Ngo

Submitted to the Department of Electrical Engineering and Computer Science
on May 28, 2007, in partial fulfillment of the
requirements for the degree of
Master of Engineering in Electrical Engineering and Computer Science

Abstract

Neuroscientists hypothesize that the pathologies of some neurological diseases are associated with neuroanatomical abnormalities. Diffusion Tensor Imaging (DTI) and stochastic tractography allow us to investigate white matter architecture non-invasively through measurements of water self diffusion throughout the brain. Many comparative studies of white matter architecture utilize spatially localized comparisons of diffusion characteristics. White matter tractography enables studies of fiber bundle characteristics. Stochastic tractography facilitates these investigations by providing a measure of confidence regarding the inferred fiber bundles. This thesis presents an implementation of an easy to use, open-source stochastic tractography system that will enable novel studies of fiber tract abnormalities. We demonstrate an application of the system on real DTI images and discuss possible studies of frontal lobe fiber differences in Schizophrenia.

Thesis Supervisor: Polina Golland
Title: Assistant Professor

Thesis Supervisor: Carl-Fredrik Westin
Title: Associate Professor

Acknowledgments

This thesis would not have been possible without the assistance, encouragement and advice of many people. I acknowledge a few below but it is by no means a complete list.

Thank you Mom and Dad, for encouraging me to always reach for my dreams while reminding me that things that are worthwhile in life don't always come easily. Thank you little brother, for reminding me to do my best and thank you older brother for inspiring me.

Thank you Polina Golland and C-F Westin for being great advisers. Your honest advice and encouragement brought out the best in me. Thank you Marc Niethammer for always being willing to lend a helping hand. Thank you Raul San-Jose Estepar for your help and example code. Thank you Gudrun Rosenberger for your help and for letting me use your label maps. Thank you Marek Kubicki for talking to me about my project and giving me ideas on how to proceed. Thank you Martha Shenton for hosting me in your lab and for giving me a chance to use my thesis work in your lab's research.

Finally, I thank all my friends for their support and encouragement. Specifically, thank you Nick Chan, Tudor Masek and Benjamin Alvarado for being great friends and roommates. You guys made my last semester at MIT amazing. Thank you Richard Sinn and Christian Deonier for hosting me in your suite during the last two weeks of school so that I could concentrate on finishing the semester and of course for being amazing friends.

Contents

List of Figures

List of Tables

Chapter 1

Introduction

Magnetic Resonance Imaging (MRI) is a valuable imaging modality for studying the brain in-vivo. We can use use MRI to differentiate between tissue types, which is useful in anatomical studies. Diffusion Tensor Imaging (DTI) provides a method to characterize white matter tracts, enabling studies of white matter architecture.

We can visualize DTI data sets using a number of methods. DTI data sets provide information about the diffusion of water at each voxel, or volume element, in the form of diffusion tensors. A popular technique to visualize these diffusion tensors is to extract fiber tracts which summarize the diffusion information across many voxels. This technique is known as DTI Tractography.

One possible method of performing tractography is to generate tracts which follow the direction of maximal water diffusion of the voxels they pass through [18, 2]. This method is known as streamline tractography. However, this method does not provide information about the uncertainty of the generated tracks due to noise or insufficient spatial resolution. Stochastic white matter tractography methods try to address this problem by performing tractography under a probabilistic framework. Stochastic methods provide additional information that enables clinical researchers to perform novel studies. Several formulations of probabilistic tractography have been suggested [4, 3, 22, 11, 17], however tools which enable widespread adoption of stochastic tractography in clinical studies are not currently available. This thesis implements an easy to use system for performing stochastic white matter tractography

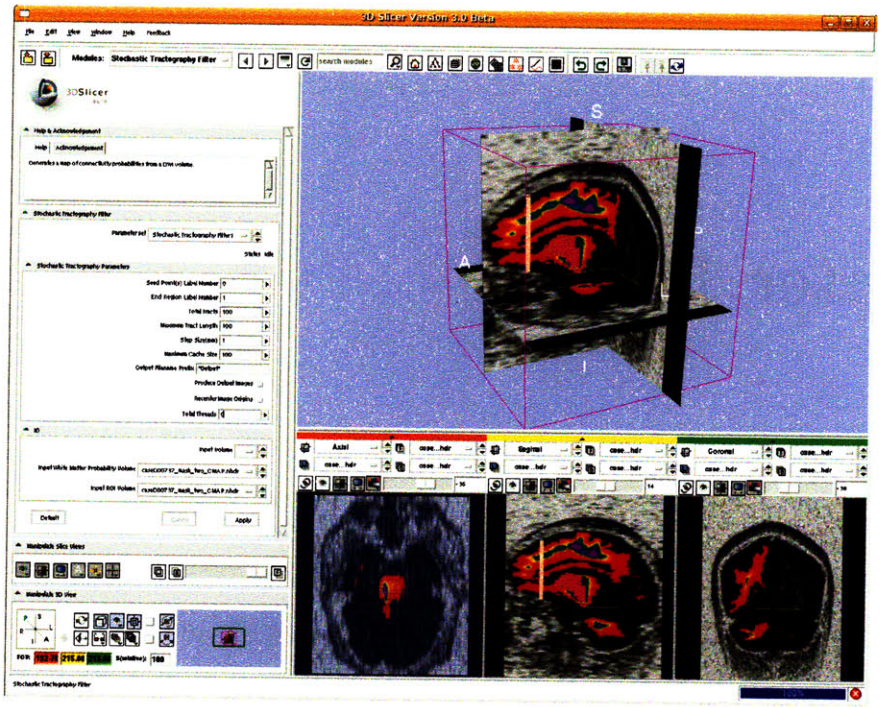

Figure 1-1: 3D Slicer environment displaying the Stochastic Tractography Module interface and a connectivity map overlaid on a fractional anisotropy image.

based on the algorithm described by Friman et al. [8, 9].

Researchers have hypothesized that white matter abnormalities may underlie some neurological conditions. For instance, people characterize schizophrenia by its behavioral symptoms. These symptoms include auditory hallucinations, disordered thinking and delusion [16]. Studies have suggested that these behavioral symptoms have some connection with the neuroanatomical abnormalities observed in schizophrenia patients[16]. Researchers can noninvasively investigate the relationship between brain white matter abnormalities and schizophrenia by using white matter tractography.

Ultimately the success of the system developed in this thesis will depend on its use in the research community. To this end, we implement the system within the open source ITK Segmentation and Registration Toolkit [7] framework. ITK is currently used in many medical data processing applications. ITK's large existing user base will encourage the system's use in the research community. Additionally, implementing the stochastic tractography algorithm within ITK facilitates its integration into the 3D Slicer [5] for medical data visualization environment. This thesis also implements

a 3D Slicer graphical user interface module for the stochastic tractography system, increasing its ease of use and further encouraging its application in clinical research (figure 1-1).

Finally, we have applied this system towards the analysis of real DTI data. Originally, the data was investigated using non-stochastic tractography methods. We present a new analysis of the data using the system implemented in this research. We also compare and contrast the results obtain from stochastic tractography and non-stochastic methods.

In this thesis we describe the motivation and implementation of the stochastic tractography system followed by a demonstration of possible applications of the system. The next chapter provides a background on nerve fiber tracts, DTI and prior work in white matter tractography. After the background, the following chapter provides a detailed explanation of the stochastic tractography algorithm. Then, we describe the implementation of the algorithm within the ITK framework and optimizations used to improve performance. Next, we demonstrate the system through an example analysis of frontal lobe nerve fiber bundles. We conclude by discussing a potential study enabled by the algorithm.

Chapter 2

Background

Diffusion Tensor Imaging (DTI or DTMRI) is a recently developed Magnetic Resonance (MR) technique that provides information about the diffusion of water molecules in the brain. In white matter, due to the interactions between water molecules and the surrounding nerve fibers, the principal diffusion direction is aligned with the local fiber orientation.

White matter tractography is a visualization and analysis tool for DTI data. It takes local diffusion information provided by DTI images and produces explicit representations of fiber bundles which may explain the observed global diffusion distribution. White matter tractography characterizes fiber bundles in-vivo and provides insights into questions concerning white matter architecture.

A number of clinical studies have used tractography to compare fiber bundle characteristics in different populations. Many of these studies utilize tractography methods which do not provide a measure of the confidence regarding the estimated fiber bundles. The stochastic tractography system implemented in this research provides these measures of confidence, and may open new avenues of clinical investigation of white matter architecture.

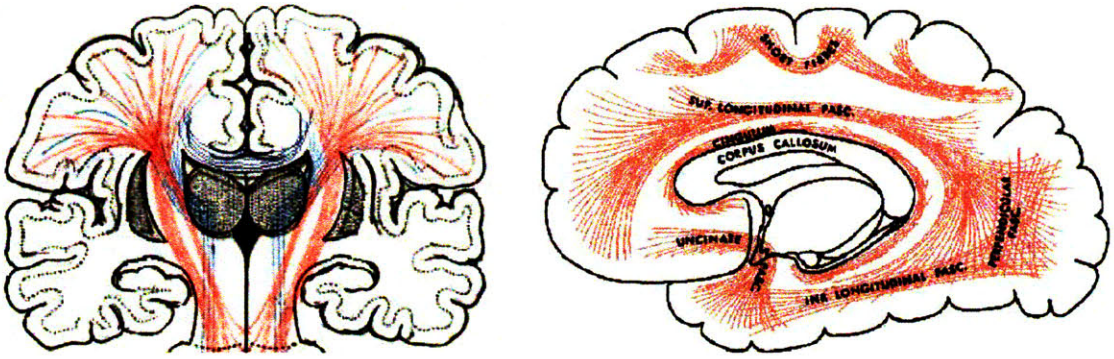

Figure 2-1: Example of human brain fiber tracts viewed from the front (coronal) and from the left (sagittal). This image was derived from anatomical atlas diagrams in Gray's Anatomy [19].

2.1 Neuroanatomy and Fiber Tracts

Nerve tissue in the brain can be divided into gray and white matter. Gray matter is found throughout the brain but is concentrated on the cortical surface as well as in structures deep within the brain such as the thalamus. The defining characteristic of gray matter is its lack of myelinated axons. In contrast, white matter is white in color because it has an abundance of myelinated axons. Myelin consists mostly of lipids and gives white matter its color. Bundles of these axons comprise white matter tracts. Figure 2-1 illustrates some prominent fiber tracts.

2.2 Diffusion Tensor MRI Physics

MRI is typically used to differentiate between different tissue types, such as gray and white matter. This technique works by magnetically polarizing a particular slice of the brain. A strong uniform magnetic field is applied to the entire brain causing the spins of the water molecules to orient in the same direction. Another magnetic field, this one nonuniform in space, polarizes the spins of the atoms in the brain differently depending on their location. This gradient field is turned off and as the spins of the electrons reorient, or relax, back to the strong uniform field, they release an electro-magnetic signal which is picked up by the receiving coil. The

frequency of these emitted waves depends on the atom's polarization which in turn depends on its position in space. The time needed for the spins to relax, known as the relaxation time, depends on the type of tissue. Using this data, an image can be constructed that differentiates between tissue types due to their characteristic relaxation time. Unfortunately, white matter appears homogeneous in anatomical MRI images. Anatomical MRI images do not provide much information about the orientation of the white fiber tracts within each voxel. Without this information it is not possible to reliably determine the connectivity between different regions of gray matter. Diffusion Tensor Imaging is a recently developed MR technique which provides more information to characterize fiber tracts.

Diffusion Tensor Imaging (DTI) or DTMRI is an imaging technique that indirectly provides information about fiber tract orientation from the diffusion profile of water in the brain tissues. Diffusion in many parts of the brain occurs anisotropically; the rate of diffusion varies with direction. This anisotropy is caused by local physical constraints that impede diffusion. The diffusion of water molecules, which are the predominant signal emitters in MR imaging, is believed to be constrained by the myelin that surrounds axons. DTI images describe the diffusion profile of water within each voxel using a diffusion tensor. These tensors can be modeled as ellipsoids with the eigenvectors describing the major and minor axes of the ellipsoid and the associated eigenvalues scaling these axes. Isotropic diffusion profiles result in spherical tensors while anisotropic diffusion profiles produce more eccentric tensors. The parameters which describe these tensors are obtained from Diffusion Weighted Images (DWI) of the same volume captured using at least six unique gradient directions and one reference image obtained in the absence of weighting gradients.

Each Diffusion Weighted Image (DWI) provides information about the magnitude of diffusion in one particular direction. Diffusion Weighted imaging works similarly to anatomical MRI imaging but it also captures the Brownian diffusion of molecules during the imaging process. Unlike anatomical MRI, an additional gradient magnetic field is applied in a chosen direction which then makes the resulting observations sensitive to the self diffusion of water in that direction. An MRI image obtained using

these diffusion sensitizing gradients is referred to as a Diffusion Weighted Image or DWI. Associated with each of these images is the direction of the magnetic field gradient used to polarize the molecules. This information is necessary because different magnetic field gradients may result in significantly different DWI images due to the anisotropy of diffusion in certain regions of the brain. Finally, this diffusion information can be used to estimate the parameters of a diffusion tensor which is then used to infer the orientation of fiber tracts in that voxel.

2.3 Diffusion Tensor

The diffusion tensor is a 3x3 symmetric matrix which describes the distribution of diffusion within each voxel. Under ideal, noise-free conditions, the diffusion tensor is related to the DWI intensity by the observation model:

$$z_i = z_0 e^{-b_i \mathbf{g}_i^T \mathbf{D} \mathbf{g}_i} \tag{2.1}$$

where $\mathbf{D}$ is the diffusion tensor, z_i is the DWI intensity, z_0 is the baseline intensity given by the B0 image, $\mathbf{g}_i$ and b_i are the associated magnetic gradient directions and diffusion weighting factor respectively.

The diffusion tensor is positive definite, thus all of its eigenvalues are positive. Each eigenvalue represents the magnitude of diffusion in the direction of the eigenvector associated with that eigenvalue. The diffusion distribution described by the tensor can be visualized as an ellipsoid, whose major and minor axis are described by the eigenvectors and associated eigenvalues of the tensor. The eigenvector associated with the largest eigenvalue is sometimes referred to as the principal diffusion direction. If the diffusion is sufficiently anisotropic, the principal diffusion direction is a good estimate of the local fiber orientation [6].

The diffusion tensor is sensitive to changes in the orientation of the object being scanned. Thus clinical studies tend to use statistics which are invariant to changes in orientation. The most commonly used properties are the trace and the fractional

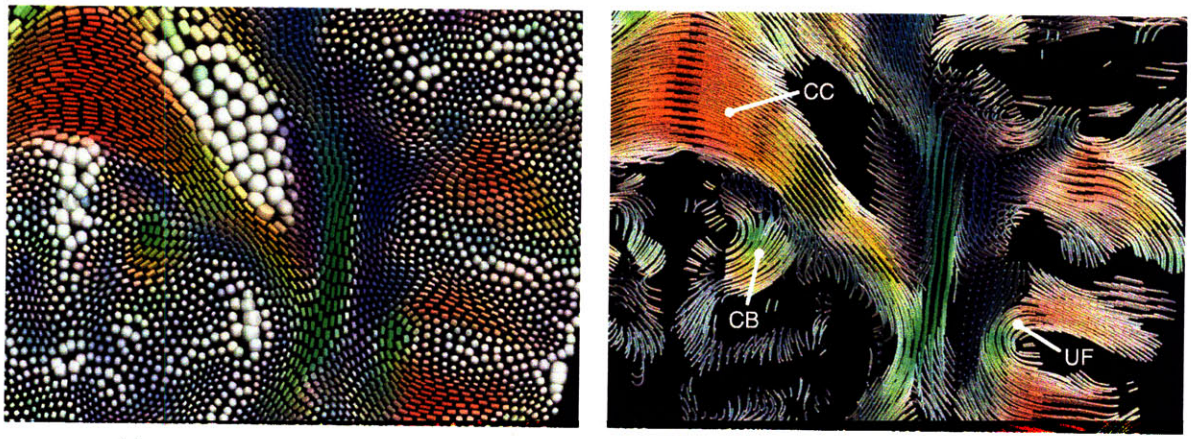

(a) superquadric tensor glyphs

(b) streamline tractography

Figure 2-2: Glyphs and streamlining tractography on the same DTI data [12]. The color in both images represent the estimated orientation of the fiber tract modulated by the degree of anisotropy in the data. The color key is red is for left-right, blue for superior-inferior, green for anterior-posterior. Regions that are white have low anisotropy while saturated regions exhibit highly anisotropic diffusion.

anisotropy. The trace of the tensor is the sum of the diagonal elements of the tensor and represents the average total diffusion. A higher trace implies that there are few obstacles to water diffusion in that voxel. Fractional anisotropy is a measure of the degree of difference between the largest eigenvalue and the smaller two eigenvalues:

$$FA = \sqrt{\frac{3[(\lambda_1 - D_{av})^2 + (\lambda_2 - D_{av})^2 + (\lambda_3 - D_{av})^2]}{2(\lambda_1^2 + \lambda_2^2 + \lambda_3^2)}} \tag{2.2}$$

$$D_{av} = \frac{\lambda_1 + \lambda_2 + \lambda_3}{3} \tag{2.3}$$

where $\lambda_1, \lambda_2, \lambda_3$ are the eigenvalues of the diffusion tensor and D_{av} FA ranges from 0 for perfectly isotropic diffusion, a sphere, to 1 for perfectly anisotropic diffusion, an infinite cylinder. While many other measures of anisotropy exist, fractional anisotropy is currently the most popular.

The two primary ways to visualize DTI data is through the use of glyphs and tractography. Figure 2-2 demonstrates these two methods. Glyphs are visual representations of the tensors at each voxel in one slice of DTI data. For instance, direct renderings of the diffusion tensor can be used as glyph. Glyph visualization is used

for understanding diffusion in a localized region of interest. Studies that investigate local differences in DTI observations between different subjects are known as Region of Interest or ROI studies. Although ROI analysis is straightforward, it is limited in the information it can provide and may actually introduce errors. For instance, it is difficult to determine if the observed location along a fiber bundle in one patient corresponds to the observed location in another patient. Ultimately, clinical researchers are often interested in the global fiber bundles which produced these local DTI observations. The fiber bundles span multiple voxels, limiting the usefulness of glyph visualization in global studies of fiber bundle characteristics. These inquiries into the characteristics of fiber bundles led to the invention of white matter tractography methods. In contrast to glyph visualization, white matter tractography incorporates diffusion information across multiple voxels in order to estimate a fiber bundle or bundles which could explain the observed diffusion data.

2.3.1 Streamline Tractography

Tractography can be performed in a number of ways. One method is to estimate tracts which are collinear with the principal direction of diffusion direction of every voxel it passes through. These methods are collectively known as streamlining methods and have been suggested and characterized by a number of researchers [18, 2]. Streamline tractography has relatively low computational cost and is very useful for visualization of DTI data. However, streamline approaches do not provide information regarding the certainty of the estimated fiber tracts, limiting their usefulness in clinical studies which investigate white matter architecture characteristics. Additionally, this lack of confidence information limits the regions that streamlining tractography can analyze. Fiber orientation in highly isotropic regions are very uncertain. Since streamlining methods do not account for this uncertainty, one cannot confidently analyze a region containing isotropic voxels using streamlining methods. To reflect this limitation, many streamline methods will not estimate tracts that even momentarily pass through isotropic regions. Unfortunately, isotropic voxels occur throughout the brain, even in regions with highly coherent fibers. These voxels appear isotropic

due to noise, distortions in the DTI data or due to limitations in imaging resolution which result in partial volume effects. Partial volume effects occur when multiple fibers cross within a single voxel resulting in a diffusion distribution which is affected by both fiber orientations. Under a single fiber observation model, partial volume effects result in reduced anisotropy and thus increased uncertainty in the fiber orientation estimate. This lack of robustness limits the method's application in studies of fiber bundle characteristics. These limitations motivated the invention of stochastic or probabilistic tractography algorithms. This class of tractography algorithms overcomes the shortcomings of streamline methods by explicitly modeling the uncertainty in the local fiber orientation.

2.3.2 Stochastic Tractography

Stochastic tractography, sometimes known as probabilistic tractography, differs from streamlining methods in that it takes into account the uncertainty in fiber orientation when calculating estimates of fiber tracts. Stochastic methods perform tractography under a probabilistic framework; beliefs regarding the estimated local fiber orientation are propagated to provide a measure of confidence regarding fiber tracts that span multiple voxels. This explicit modeling and propagation of beliefs allows stochastic methods to generate tracts in regions of low anisotropy. Stochastic methods can generate tracts that momentarily pass through regions of low anisotropy because they integrate local fiber orientation uncertainty into the uncertainty of the entire tract. The robustness of stochastic methods to local fiber orientation uncertainty has even enabled some studies to directly assess the connectivity of gray matter, which generally exhibits isotropic diffusion, with other regions of the brain[3].

Bootstrap Method

The Bootstrap Method is a stochastic method that calculates the degree of connectivity between different regions of the brain based on the variance in the original DTI data. The method obtains a measure of the variance of the DTI data by using

redundant sets of DTI data and through the creation of new data which consist of recombinations of the original data. In Jones et al. [11] nine redundant sets of DWI volumes are obtained to perform the Bootstrap method. Random combinations of portions of DWI volumes are sampled from this pool to generate a large number of complete mixed DWI sets known as bootstraps. These complete mixed DWI sets are then converted to DTI images. Standard streamline tractography is then performed on each bootstrap set at the same starting, or seed location. A visitation percentage is then calculated for each voxel in the volume indicating the percentage of sample sets which generated a tract that passed through that particular voxel. This visitation percentage can be interpreted as the probability that a voxel is connected to the seed point via a fiber tract.

Bayesian Methods

Stochastic tractography methods which use Bayesian frameworks express beliefs about estimated fiber tracts by generating a posterior probability distribution of fibers given the observed DTI data. These tractography methods use a probabilistic model to relate the underlying fiber orientation with the observed DTI data. The probabilistic model is applied to every voxel to generate a posterior distribution of possible fiber orientations given the observed diffusion in that voxel. A streamline-like tractography method is then used to generate tracts by randomly sampling fiber directions from the fiber orientation posterior at each voxel as calculated by the local model. The sampled tract is a realization of a random variable generated from the posterior distribution of fibers. Since there are many possible paths, to obtain a good approximation of the posterior distribution, many paths must be sampled. Additionally, similar to the Bootstrap method, the probability that region A is connected to region B can then be found by calculating the fraction of paths that pass through region B originating from A.

Behrens's Bayesian approach was one of the pioneering works in the field of stochastic tractography[3]. An important idea in Behren's work is in keeping clear the distinction between estimating a general diffusion distribution from DWI data

and estimating the local fiber orientation from DWI data. Although an inference of the local fiber orientation can be made from the tensor model's principal diffusion direction, the tensor model is primarily a model to infer the distribution of diffusion given the data. However, in stochastic tractography, we wish to infer the local fiber orientation from the observed diffusion data. Behrens's formulates this distinction by avoiding the tensor model altogether in favor of the two-compartment model. The two-compartment model makes the assumption that only a single fiber passes through a voxel. Deviations from this simple model due to crossing fibers is captured as uncertainty in the fiber orientation. In this model a voxel is described as two compartments whose net diffusion profile is the sum of a small anisotropic diffusion component that occurs in and around the fiber and a larger isotropic diffusion component outside of the fiber [3]. The fiber orientation distribution is analytically intractable. Behrens overcomes this issue by computing the PDF using Markov Chain Monte Carlo (MCMC) techniques [1]. MCMC is a method to numerically integrate an analytically intractable integral. Unfortunately, MCMC methods are sometimes computationally expensive. Thus Friman et al. [9] introduced a stochastic method that avoids MCMC. Our system implements a stochastic tractography method based on Friman's approach. In the next section, we provide a detailed explanation of the theory behind the stochastic tractography algorithm implemented in this thesis.

Chapter 3

Stochastic Tractography Algorithm

The stochastic tractography algorithm implemented in this thesis is based on Friman's [9] approach with some modifications to the stopping criteria. Figure 3-1 provides a flow chart demonstrating key steps in the algorithm.

A fiber tract is modeled as a sequence of unit vectors. The orientation of these unit vectors is determined by sampling a posterior fiber orientation distribution which is dependent on the local diffusion data as well as the orientation of the unit vector in the previous step. The posterior distribution is a normalized product of the prior likelihood of the fiber orientation and the likelihood of that fiber orientation given the local diffusion data.

Friman uses a subset of the tensor model which is called a constrained diffusion model. In this model, the two smallest eigenvectors of diffusion tensor are equal, constraining the shape of the diffusion tensor to be linearly anisotropic. The constrained model rules out the possibility of nonlinear, or non-cylindrical anisotropic diffusion distributions. Deviations from linearly anisotropic diffusion distributions are captured as uncertainty in the fiber orientation. The constrained model is combined with a Gaussian DWI noise model to obtain a fiber orientation likelihood function. The parameters for the constrained model are derived from a weighted least squares estimation of the parameters for the log tensor model.

The orientation of each vector depends only on the previous vector. This dependency is formulated in the prior on the fiber orientation. Prior knowledge about

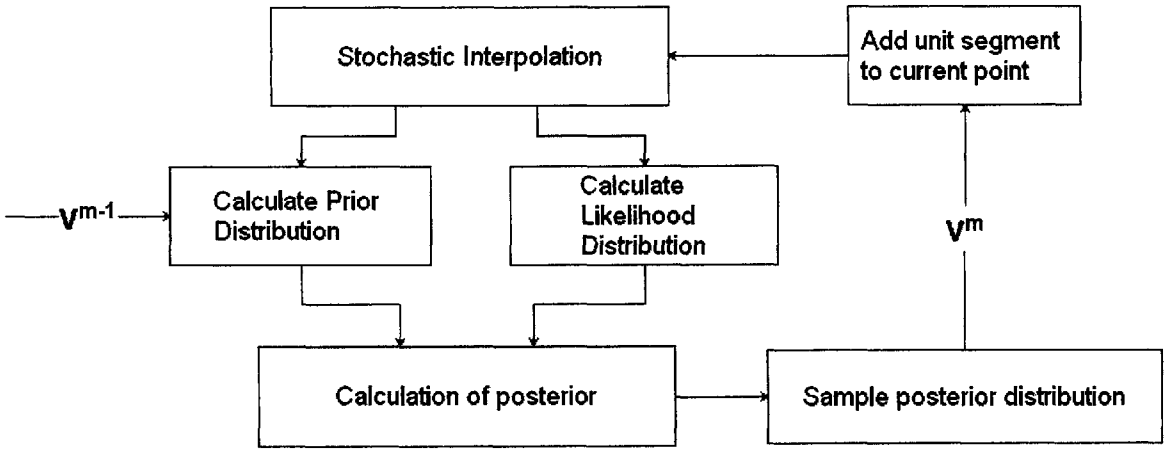

Figure 3-1: A flow chart demonstrating key steps in the stochastic tractography algorithm

the regularity of the fiber tract can encoded in this prior probability. The prior also serves to prevent the fiber from backtracking, since the likelihood distribution alone is axially symmetric.

Friman's approach is a Bayesian inference algorithm similar to Behrens's but with some important optimizations [9]. In contrast with Behrens's two-compartment observation model, the constrained model used by Friman is derived from the thoroughly studied tensor model of diffusion. The advantage of using the constrained model is that it is relatively easy to estimate the parameters for the model. The parameters for the constrained model are obtained after the tensor model has been fit to the diffusion data. Since the parameters for the tensor model are easily obtained through many computationally efficient ways, the constrained model's parameters are likewise easy to obtain. The constrained model can be fit to every voxel within a matter of seconds whereas Behrens's model takes a couple of hours [9]. Additionally Friman avoids using MCMC techniques by assuming that parameters other than the principle diffusion direction take on their ML estimates with certainty within each voxel. Friman demonstrates that eliminating this source of uncertainty has little effect on the resulting posterior fiber orientation distribution.

In Friman's paper on stochastic tractography, the tracking is terminated when an encountered voxel's diffusion distribution below a minimal measure of anisotropy. However, since the stochastic tractography algorithm takes into account this uncer-

tainty with an increase in the spatial variance of sampled fibers, this termination criterion seems arbitrary and contradictory with the goals of stochastic tractography, which is to enable sampling of tracts in regions of uncertainty. Thus we replace this termination criterion with one which terminates tractography based on the posterior probability that a fiber tract exists within the current voxel. The posterior probability that a fiber tract exists in a given voxel can be obtained by performing a soft segmentation of white matter on an anatomical image co-registered with the DWI data. Alternatively, the soft segmentation can also be performed on the B0 image of the DWI data set, thus eliminating the need for additional data. While this may seem equivalent to using an anisotropy threshold criterion, since white matter generally has higher anisotropy than gray matter, it does not exclude regions of white matter which have low anisotropy due to crossing fibers. This criteria should enable the algorithm to detect more tracts than under the anisotropy termination criteria.

3.1 Mathematical Derivation

3.1.1 Linearized Diffusion Tensor Model

For each voxel in the DWI volume a signal intensity z_i can be measured given a particular diffusion weighting factor b_i and magnetic gradient direction $\mathbf{g}_i = (g_{ix} \quad g_{iy} \quad g_{iz})^T$. The subscript i enumerates multiple measurements of the same voxel under different magnetic gradient directions.

The tensor model is a popular model used to describe the relationship between a particular gradient direction $\mathbf{g}_i$, the diffusion weighting factor b_i and the measured voxel intensity z_i:

$$z_i = z_0 e^{-b_i \mathbf{g}_i^T \mathbf{D} \mathbf{g}_i} \tag{3.1}$$

$$\mathbf{D} = \begin{pmatrix} D_{xx} & D_{xy} & D_{xz} \\ D_{xy} & D_{yy} & D_{yz} \\ D_{xz} & D_{yz} & D_{zz} \end{pmatrix} \tag{3.2}$$

where $\mathbf{D}$ is the diffusion tensor, encoded as a 3×3 matrix that describes the rate of diffusion in 3D space.

Taking the log of both sides of the equation leads to a more tractable linear relationship:

$$\log(z_i) = \log(z_0) - b_i \mathbf{g}_i^T \mathbf{D} \mathbf{g}_i \tag{3.3}$$

The model is now in a linear form so that we can apply standard techniques such as least squares to estimate the diffusion parameters (the entries of the $\mathbf{D}$). The linearized form can be further simplified by expanding the matrix multiplications and isolating the parameters into a separate vector.

$$\log(z_i) = \mathbf{a}_i^T \mathbf{q} \tag{3.4}$$

$$\mathbf{a}_i = \begin{pmatrix} 1 & -b_i g_{ix}^2 & -b_i g_{iy}^2 & -b_i g_{iz}^2 & -2b_i g_{ix} g_{iy} & -2b_i g_{ix} g_{iz} & -2b_i g_{iy} g_{iz} \end{pmatrix}^T \tag{3.5}$$

$$\mathbf{q} = \begin{pmatrix} z_0 & D_{xx} & D_{yy} & D_{zz} & D_{xy} & D_{xz} & D_{yz} \end{pmatrix}^T \tag{3.6}$$

The entries of the diffusion tensor $\mathbf{D}$ and the scaling factor z_0 now correspond to entries in the $\mathbf{q}$ vector.

There are 7 parameters that must be solved for in $\mathbf{q}$. At least 6 additional independent equations are required in order to solve for the parameters. These equations can be obtained by measuring the voxel intensity using at least 7 noncolinear gradient directions g_i and optionally by varying the diffusion weighting factor b_i. However, more than 7 directions are required to estimate the variance of the original data, as we discuss later in this section. The full system of equations containing all n measurements of a voxel can be succinctly represented in matrix form:

$$\log(\mathbf{z}) = \mathbf{A}\mathbf{q} \tag{3.7}$$

Where $\mathbf{A}$ is a $n \times 7$ matrix and $\log(\mathbf{z})$ is an n length vector of the n voxel intensities. The least squares solution has the following form:

$$\hat{\mathbf{q}} = (\mathbf{A}^T\mathbf{A})^{-1}\mathbf{A}^T \log(\mathbf{z}) \tag{3.8}$$

3.1.2 Constrained Diffusion Tensor Model

Although the tensor model provides a good description of a general diffusion profile, ultimately we would like to estimate the distribution of the fiber orientations from the voxel intensities. To simplify the tractography process we assume that each voxel contains only one fiber, and the majority of diffusion occurs in the single direction dictated by this single fiber. The assumption is mathematically modeled by constraining the diffusion tensor to forcing the two smallest eigenvalues to be equal. Under this constraint the eigen-decomposition of the diffusion tensor $\mathbf{D}$

$$\mathbf{D} = \lambda_1 \hat{\mathbf{e_1}}\hat{\mathbf{e_1}}^T + \lambda_2 \hat{\mathbf{e_2}}\hat{\mathbf{e_2}}^T + \lambda_3 \hat{\mathbf{e_3}}\hat{\mathbf{e_3}}^T \tag{3.9}$$

is simplified by assuming the two smallest eigenvalues $\lambda_2 = \lambda_3 = \alpha$:

$$\begin{aligned} \mathbf{D} &= \lambda_1 \hat{\mathbf{e_1}}\hat{\mathbf{e_1}}^T + \alpha(\hat{\mathbf{e_2}}\hat{\mathbf{e_2}}^T + \hat{\mathbf{e_3}}\hat{\mathbf{e_3}}^T) \\ &= (\lambda_1 - \alpha)\hat{\mathbf{e_1}}\hat{\mathbf{e_1}}^T + \alpha\mathbf{I} \\ &= \beta\hat{\mathbf{e_1}}\hat{\mathbf{e_1}}^T + \alpha\mathbf{I} \end{aligned} \tag{3.10}$$

Substituting this expression into the tensor model in equation(3.1) yields the constrained model:

$$z_i = z_0 e^{-\alpha b_i} e^{-\beta b_i (g_i^T \hat{\mathbf{v}})^2} \tag{3.11}$$

where $\hat{\mathbf{v}}$ represents $\hat{\mathbf{e_1}}$, the eigenvector associated with the largest eigenvalue. This change emphasizes that the constrained model attempts to model the underlying fiber orientation and not the general diffusion profile.

The parameters of the constrained model can be derived from the parameters of the tensor model. Given matrix $\mathbf{D}$ with the eigenvalue factorization of equation (3.9), the closest symmetric matrix, in terms of the Frobenius norm , with the two equal smallest eigenvalues is [9]:

$$\mathbf{S} = \lambda_1 \hat{\mathbf{e_1}} \hat{\mathbf{e_1}}^T + \frac{\lambda_2 + \lambda_3}{2}(\hat{\mathbf{e_2}} \hat{\mathbf{e_2}}^T + \hat{\mathbf{e_3}} \hat{\mathbf{e_3}}^T) \tag{3.12}$$

Hence after fitting the tensor model we obtain the constrained model parameters:

$$\alpha = \frac{\lambda_2 + \lambda_3}{2},\ \beta = \lambda_1 - \alpha,\ \hat{\mathbf{v}} = \hat{\mathbf{e}} \tag{3.13}$$

The additional constraints imposed by the constrained model reduces the goodness of fit, as compared to the diffusion tensor model, for voxels that do not exhibit anisotropic diffusion. The reduction in anisotropy may be due to partial volume effects and the constrained model captures this uncertainty with an increase residual variance which translates into a wider fiber orientation likelihood function.

3.1.3 Fiber Orientation Likelihood Function

The log of the measured voxel intensity can be described as the log of the true intensity z_i with some additive noise ϵ:

$$y_i = \log(z_i) + \epsilon_i \tag{3.14}$$

For moderate levels of SNR, Salvador et al. [21] demonstrates that the distribution of the noise (3.14) is approximately normal with a mean of zero and a variance equal to the variance of the original complex data [21], divided by the square of the non-log noise-free voxel intensity:

$$p(\epsilon_i) = N\left(0, \frac{\sigma_i^2}{z_i^2}\right) \tag{3.15}$$

Therefore the resultant distribution of the log of the measured voxel intensity can be modeled by the same normal distribution, whose mean has been shifted by the log of

the noise-free intensity:

$$p(y_i) = N\left(\log(z_i), \frac{\sigma_i^2}{z_i^2}\right) \tag{3.16}$$

The joint distribution of the n noisy voxel log-intensities is obtained by multiplying the n distributions together. It is assumed that the variance of the original complex data is constant across all n measurements of a voxel.

$$p(\mathbf{y}) = \prod_{i=1}^{n} N\left(\log(z_i), \frac{\sigma^2}{z_i^2}\right) \tag{3.17}$$

In other words, equation (3.17) is the likelihood of observing the measured data given the noise-free intensities z_i. Since we cannot directly observe z_i we estimate them by fitting parameters for the constrained model from the observed noisy data $\mathbf{y}$. Hence, after substituting in the constrained model, z_i becomes $\hat{z}_i$ and equation (3.17) becomes the likelihood of observing the measured data given a choice of parameters for the constrained model. Since the parameter of primary interest is the estimated fiber direction $\hat{\mathbf{v}}$, it is separated from the estimated secondary parameters $\hat{\theta} = \{\hat{z}_0, \hat{\alpha}, \hat{\beta}, \hat{\sigma}^2\}$. σ^2 is the variance of the original complex data [21], not the variance of the intensity z_i. It can be estimated by calculating the residual variance after fitting the parameters of the constrained model.

$$\hat{\sigma}^2 = \frac{(\log(\mathbf{y}) - \mathbf{A}\hat{\mathbf{q}})^T(\log(\mathbf{y}) - \mathbf{A}\hat{\mathbf{q}})}{n-7} \tag{3.18}$$

$$p(\mathbf{y}|\hat{\mathbf{v}}, \hat{\theta}) = \prod_{i=1}^{n} N\left(\log(\hat{z}_i), \frac{\hat{\sigma}^2}{\hat{z}_i^2}\right) \tag{3.19}$$

3.1.4 Connectivity Probability Function

A generated fiber tract k of length l can be modeled as string of l unit vectors lined end to end: $\mathbf{v}_{k,1:l} = \{\hat{\mathbf{v}}_1, \ldots, \hat{\mathbf{v}}_l\}_k$. Ω_A^l is the set of all possible l length paths that originate from point A. A probability function can be defined on the path space for l length paths: $p(\mathbf{v}_{k,1:l})$ and consequently $p(\Omega_A^l) = 1$. Additionally, a discrete probability function $p(l)$ can be defined on the path length. Given the diffusion measurements

$\mathbf{y}$, the probability that region A is connected to region B by a fiber tract, assuming that the path length is independent of the diffusion measurements is:

$$p(A \rightarrow B|\mathbf{y}) = \sum_{l=1}^{\infty} \int_{\Omega_{AB}^{n}} p(l)p(\mathbf{v}_{1:l}|\mathbf{y}) \tag{3.20}$$

In general, equations such as (3.20) which contain multidimensional integrals over complex path spaces are not tractable analytically and must be calculated numerically. The equations below provide a method to approximate equation (3.20) numerically. N_l paths of length l are sampled from the path space Ω_A^l. $\mathbb{I}$ is an indicator function that takes on the value 1 only if a particular l length path $\mathbf{v}_{1:l}^k$ originating from region A passes through region B, and is 0 otherwise. The indicator function is used to calculate the fraction of sampled paths originating in region A that pass through B, of a particular length l. Finally, these fractions are weighted by the probability of the path length $p(l)$ and summed over all possible path lengths. The infinite summation over path length converges because there is a maximum path length beyond which longer lengths have zero probability.

$$\mathbb{I} = \begin{cases} 1 & \mathbf{v}_{k,1:l} \in \Omega_{AB}^{n} \\ 0 & \text{otherwise} \end{cases} \tag{3.21}$$

$$p(A \rightarrow B|Y) \approx \sum_{l=1}^{\infty} \sum_{k=1}^{N_n} p(l) \frac{\mathbb{I}(\mathbf{v}_{k,1:l})}{N_n} \tag{3.22}$$

3.1.5 Stochastic Fiber Tract Generation

According to equation (3.22), we must randomly sample tracts originating from region A. These tracts can be generated stochastically, in the sense that the tract can be generated from repeated samples from a probability distribution. In this case we are drawing from the distribution of fiber orientations at a given point in space. This prior distribution can be refined by incorporating likelihood information from the constrained model, as well as prior information regarding the regularity of the fiber tract, to generate a posterior fiber orientation distribution.

$$p(\hat{\mathbf{v}}_i, \theta|\hat{\mathbf{v}}_{i-1}, \mathbf{y}) = \frac{p(\mathbf{y}|\hat{\mathbf{v}}_{i-1}, \hat{\mathbf{v}}_i, \theta)p(\hat{\mathbf{v}}_i, \theta|\hat{\mathbf{v}}_{i-1})}{p(\mathbf{y}|\hat{\mathbf{v}}_{i-1})} \tag{3.23}$$

Assuming the secondary parameters θ at the current point are independent of the previous step direction and prior knowledge about the next step direction: $p(\hat{\mathbf{v}}_i, \theta|\hat{\mathbf{v}}_{i-1}) = p(\hat{\mathbf{v}}_i|\hat{\mathbf{v}}_{i-1})p(\theta)$ and assuming diffusion measurements at the current point don't depend on the previous step direction: $p(\mathbf{y}|\hat{\mathbf{v}}_{i-1}, \hat{\mathbf{v}}_i, \theta) = p(\mathbf{y}|\hat{\mathbf{v}}_i, \theta)$ and $p(\mathbf{y}|\hat{\mathbf{v}}_{i-1}) = p(\mathbf{y})$ equation (3.23) simplifies:

$$p(\hat{\mathbf{v}}_i, \theta|\hat{\mathbf{v}}_{i-1}, \mathbf{y}) = \frac{p(\mathbf{y}|\hat{\mathbf{v}}_i, \theta)p(\hat{\mathbf{v}}_i|\hat{\mathbf{v}}_{i-1})p(\theta)}{p(\mathbf{y})} \tag{3.24}$$

The denominator $p(\mathbf{y})$ normalizes the posterior probability distribution, allowing it to integrate to 1, and can be written as the integral of the numerator.

$$p(\mathbf{y}) = \int_{\hat{\mathbf{v}}_i, \theta} p(\mathbf{y}|\hat{\mathbf{v}}_i, \theta)p(\hat{\mathbf{v}}_i|\hat{\mathbf{v}}_{i-1})p(\theta) \tag{3.25}$$

The likelihood function $p(\mathbf{y}|\hat{\mathbf{v}}_i, \theta)$ is given by equation 3.19.

The prior probability function $p(\hat{\mathbf{v}}_i|\hat{\mathbf{v}}_{i-1})$ is used to encode knowledge about the regularity of fiber tracts:

$$p(\hat{\mathbf{v}}_i|\hat{\mathbf{v}}_{i-1}) = \frac{1}{\zeta}\begin{cases} (\hat{\mathbf{v}}_i^T\hat{\mathbf{v}}_{i-1})^\gamma & \hat{\mathbf{v}}_i^T\hat{\mathbf{v}}_{i-1} \geq 0, \\ 0 & \hat{\mathbf{v}}_i^T\hat{\mathbf{v}}_{i-1} < 0 \end{cases} \tag{3.26}$$

While data from invasive studies nerve fibers can be used to estimate this PDF, for the purposes of this implementation a simple distribution given by (3.26) where $\gamma \geq 0$ and $\frac{1}{\zeta}$ is a normalization factor that allows the distribution to integrate to 1. This particular distribution gives preference to paths which continue in the prior direction and gives zero probability to perpendicular turns. The most important function of the prior is to prevent the fiber tract from backtracking on itself. Without the prior, this may occur because the likelihood function is symmetric.

Since we want to obtain the posterior PDF for the fiber direction alone, we must marginalize the joint posterior distribution (3.24) by integrating over the secondary

parameters θ. To simplify this integration, we remove uncertainty regarding the secondary parameters, θ by assuming an ML estimate. These ML estimates were calculated by fitting the constrained model (3.13). Under this assumption equation (3.25) simplifies to an integration only over the fiber directions $\hat{\mathbf{v}}_i$. To simplify drawing samples from the posterior distribution, the continuous PDF (3.24) can by approximated by a discrete PDF as long as the continuous PDF is sampled finely enough. Friman et al. [9] found empirically that 2,562 directions spread evenly over a unit sphere S was sufficient. Taking these simplifications into account, equation (3.24) becomes:

$$p(\hat{\mathbf{v}}_i|\hat{\mathbf{v}}_{i-1}, \mathbf{y}) = \frac{p(\mathbf{y}|\hat{\mathbf{v}}_i, \theta)p(\hat{\mathbf{v}}_i|\hat{\mathbf{v}}_{i-1})}{\sum_{\hat{\mathbf{v}}\in\mathbf{S}} p(\mathbf{y}|\hat{\mathbf{v}}_i, \theta)p(\hat{\mathbf{v}}_i|\hat{\mathbf{v}}_{i-1})} \tag{3.27}$$

Finally, since the probabilistic tractography is performed in the continuous space while the diffusion data is discretized, a decision must be made about which voxel's diffusion information should be used in the calculation of the posterior PDF at the current point. This algorithm chooses an probabilistic interpolation method suggested by Behrens et al. [3] which randomly selects a voxel near the current tract generation point, with closer voxels having a higher probability of being selected.

Chapter 4

Implementation

4.1 Architecture

We implemented the algorithm as a new filter in the Insight Segmentation and Registration Toolkit (ITK). The ITK toolkit is a collection of image processing and statistical analysis algorithms for biomedical imaging applications. Additionally, the ITK toolkit is open-source software, which allows other researchers to learn directly how this system was implemented and make improvements in the future. Including the algorithm in the ITK toolkit makes it available to a large existing research community. Additionally, we created a GUI module for the 3D Slicer medical visualization program that provides easy access to the algorithm via an intuitive visual interface. We also created a command line interface to the ITK filter that can be used to process large numbers of data sets in a batch mode. Choosing to implement the algorithm as an extension of already established tools facilitates adoption of the algorithm in clinical studies.

The stochastic tractography algorithm is a Monte Carlo algorithm which samples the high dimensional parameter space of fiber tracts. This parameter space is large because fiber tract are characterized by a sequence of segment orientations, each of which can be considered a separate parameter describing the fiber tract. As such, it may take many samples to accurately approximate the posterior distribution of these parameters. However, since these samples are IID, the samples can be generated

in parallel. Implementing the system in a multithreaded fashion enables parallel sampling of the tract distribution.

ITK provides a framework for implementing multithreaded algorithms. The ITK multithreading framework assumes that the output region can be divided into disjoint sections with each thread working exclusively on their own section of the output image. This design prevents threads from simultaneously writing to the same memory region, which may cause unexpected results. However, since the stochastic tractography algorithm generates tracts that may span the entire output image, dividing the output region into disjoint sections is not possible. Additionally, in order to obtain statistics on these tracts, we need to output the generated tracts as well as the resultant connectivity image. Thus the existing ITK framework for implementing multithreaded filters is not very useful for our stochastic tractography filter. Fortunately ITK also provides basic multithreading functions which allowed us to create a custom multithreaded design for the stochastic tractography system that is still within the ITK framework.

Each thread of stochastic tractography filter is an instance of the stochastic tractography algorithm. The block diagram in figure 4-1 demonstrates graphically the architecture of the ITK stochastic tractography filter. Every thread allocates it own independent memory for the tract that it is currently generating. Once the tract has terminated, the thread stores a memory pointer to the completed tract in a tract pointer container that is shared among all threads. The tract pointer container is protected by a mutex, which serializes write operations so that only one thread can store its completed tract in the vector at a time. Once the filter has generated enough samples, the tracts can be transferred to an output image to create a connectivity map. Additionally other statistics can be computed on the tracts. In essence, we divide the process into two sections, a multithreaded portion that samples the tracts and a single threaded portion which accumulates the tracts and calculates relevant statistics on them.

The most computationally expensive part of the algorithm is the calculation of the likelihood distribution. The algorithm must compute probabilities for 2,562 possible

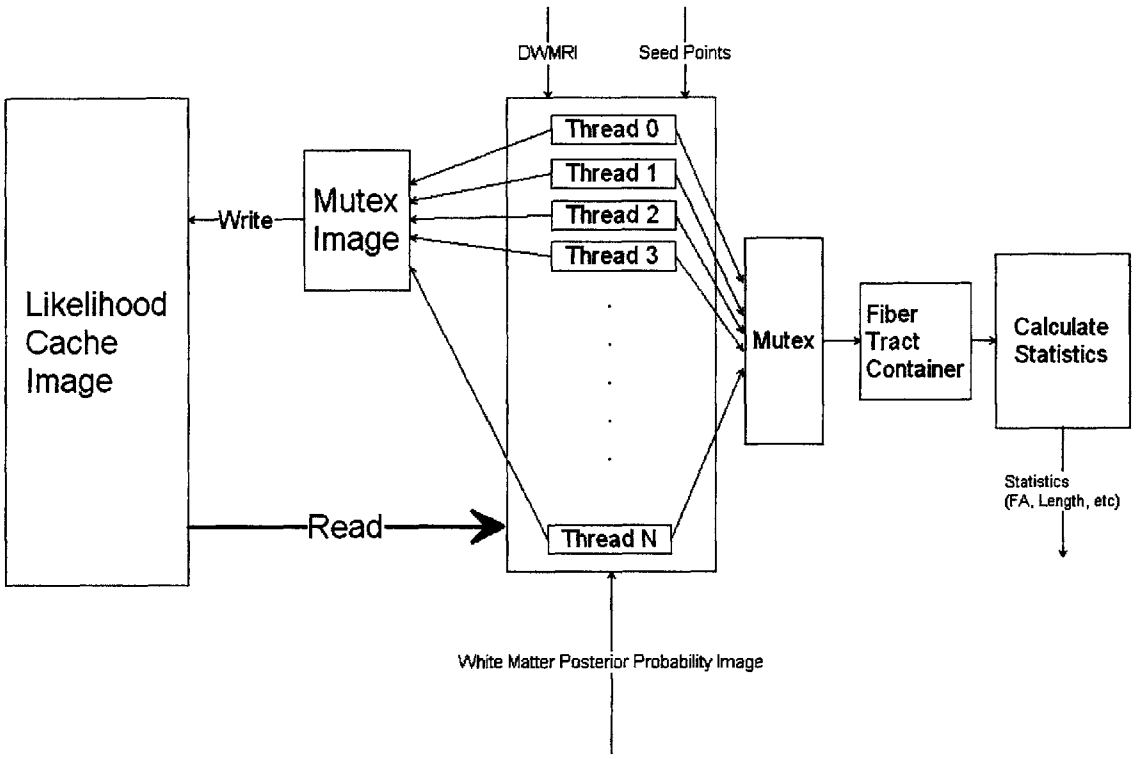

Figure 4-1: A block diagram of the filter showing its shared likelihood cache and multithreaded architecture.

fiber orientations in a voxel. Fortunately, this likelihood distribution is a deterministic function of the diffusion observations within that voxel. The filter runs much faster, at the cost of additional memory, by caching the generated likelihood distribution for later access. Caching is effective because in highly anisotropic regions of the brain, the sampled tracts are expected to be dense causing many of the sampled tracts to visit the same voxels many times.

The cache is implemented as an image whose voxels are re-sizable arrays. ITK's optimized pixel access capabilities enable quick access to the likelihood distribution associated with any voxel in the image. On creation, every voxel in the likelihood cache image is initiated to a zero length array. Whenever the algorithm encounters a voxel, it first checks to see if the likelihood cache contains this voxel by testing if associated array is zero length. If the voxel has never been visited, the associated array is resized and the computation of the likelihood distribution associated with this voxel is stored inside the newly resized array.

Using a shared likelihood cache between multiple concurrent threads creates additional complexities. Simultaneous writes to the cache would cause unexpected behavior. Additionally there is the possibility of one thread reading an incomplete cache entry while another thread is trying to write it. One possible solution is to ensure that only one thread can read or write to the likelihood cache at a time. This is easily implemented by serializing access to the likelihood cache using a mutex. A mutex serves as a lock on data. A thread will wait to obtain a lock on the data before it proceeds to the next section of code. Inside this section, which is called the critical section, the thread holds the lock ensuring exclusive access to the otherwise shared data. All other threads must wait and idle while the thread which owns the lock finishes it operations. Since threads must access the likelihood cache very often, this results in a situation where many threads are waiting for other threads to finish accessing the likelihood cache. The serialized access to the likelihood cache creates a bottleneck, which in the worse case would result in performance that is only marginally better than a single threaded version of the filter.

Access collisions to the likelihood cache can be reduced if we increase the granularity of the lock. Instead of using one large lock for the entire likelihood cache image, we use a lock for each voxel. The probability of two threads accessing the same voxel simultaneously is much less than the probability of two threads accessing any part of the likelihood cache. These per voxel locks are conveniently constructed using an ITK image whose voxel data type is a mutex. Similar to the likelihood cache, this collection of mutexes is indexed by coordinates which correspond to the coordinates of the voxels in the DWI input data. Again, access to the mutex image is fast due to ITK's optimized access operators for data types indexed by coordinates. The only cost to using this high resolution mutex image is the additional memory required to store pixel mutexes. However this cost is small since a mutex is essentially a Boolean variable. The mutex image allows different voxels in the likelihood cache image to be updated simultaneously, increasing the rate that the likelihood cache is filled. The advantage of using a mutex image is most evident when tracking in highly isotropic regions, where collisions are very unlikely to occur, since the sampled paths are very

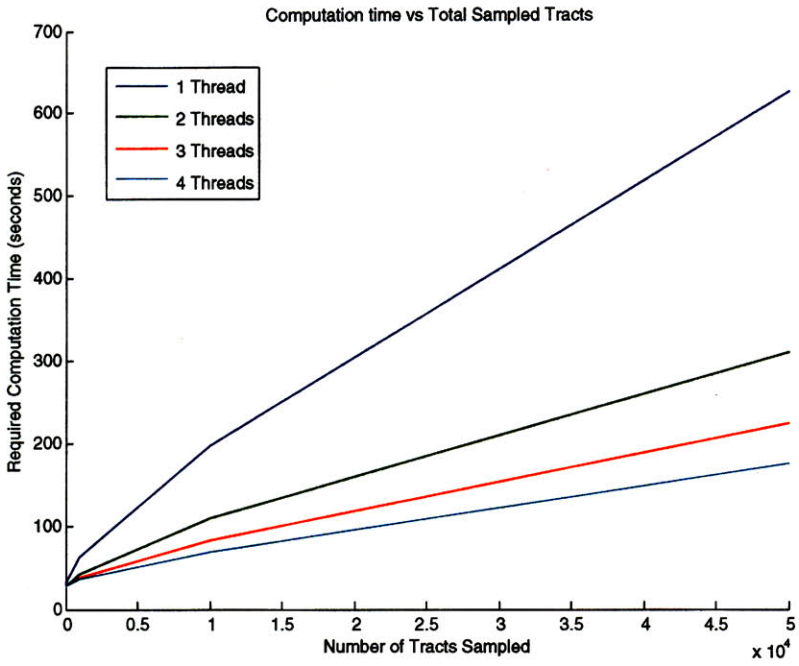

Figure 4-2: A graph displaying the amount of time needed to sample a number of tracts. Each line represents the algorithm's performance using different numbers of threads. This test was run on a 4 processor machine.

dispersed. Even on uni-processor systems, using multiple threads may improve performance since the rate of encountering an unvisited voxel may be higher, thus filling the likelihood cache faster. Figure 4-2 demonstrates the required computation time for a given number of tracts under different number of threads.

Additionally, to compute the weighted least squares estimates for the log tensor model parameters, we must first estimate the weights. These weights are found by calculating a least squares estimate of the true intensities of each voxel. The **A** matrix 3.7 used in this least squares estimation is a function solely of the magnetic gradient directions and associated b-values, which are the same for every voxel in the image. Since the same **A** matrix is used for each voxel in the least squares calculation, a common optimization is to orthogonalize the **A** matrix by computing its QR decomposition. While this operation is computationally expensive, it is performed only once for the entire DWI image. The orthogonalized **A** matrix reduces the cost of computing the weights for every voxel.

4.2 ITK Stochastic Tractography Filter

The Stochastic Tractography Filter is implemented as a multithreaded image filter in ITK under the class name itk::StochasticTractographyFilter. The filter is templated over the DWI and white matter probability map input image types and also on the connectivity map image type. The filter expects the DWI input image type to be an ITK VectorImage Type. The code below demonstrates how to instantiate the Stochastic Tractography Filter.

```
//Define Types
typedef itk::VectorImage< unsigned short int, 3 > DWIVectorImageType;
typedef itk::Image< float, 3 > WMPImageType;
typedef itk::Image< unsigned int, 3 > CImageType;
typedef itk::StochasticTractographyFilter< DWIVectorImageType, WMPImageType,
  CImageType > PTFilterType;
//Allocate Filter
PTFilterType::Pointer ptfilterPtr = PTFilterType::New();
```

The filter's required inputs and parameters must be set before it can be run. Table 4.1 lists filter methods that should be called to set the required inputs and parameters, and a short description of what each methods expects as arguments.

The code below is a continuation of the demonstration above and shows how to setup the filter's required inputs and parameters. The inputs to these methods are provided by ITK's image readers.

```
ptfilterPtr->SetInput( dwireaderPtr->GetOutput() );
ptfilterPtr->SetWhiteMatterProbabilityImageInput( wmpreader->GetOutput() );
ptfilterPtr->SetbValues(bValuesPtr);
ptfilterPtr->SetGradients( gradientsPtr );
ptfilterPtr->SetMeasurementFrame( measurement_frame );
ptfilterPtr->SetMaxTractLength( maxtractlength );
ptfilterPtr->SetTotalTracts( totaltracts );
```

Filter Member Method	Description
SetInput	DWI Image: An ITK VectorImage consisting of a vector of DWI measurements including the baseline b0 measurements, at each voxel.
SetWhiteMatterProbabilityImageInput	White Matter Probability Input: An ITK image whose voxel values range from 0 and 1 representing the posterior probability that the voxel is a white matter.
SetbValues	b-Values: An ITK VectorContainer whose elements are the corresponding b-values for the DWI input image. The b0 measurements must have a 0 b-value.
SetGradients	magnetic gradient directions: An ITK VectorContainer whose elements are 3 dimensional vnl vectors. These vectors should be unit length.
SetMeasurementFrame	DWI Measurement Frame: A 3x3 vnl matrix which transforms the gradient directions to the physical reference frame of the image. For instance multiplying a magnetic gradient direction vector by the Measurement Frame Matrix will take the vector to the RAS reference frame if RAS is the physical frame of the DWI image.
SetMaxTractLength	Maximum Tract Length: A positive integer that sets the maximum length of a sampled tract. This can also be interpreted as the number of segments which comprise the tract when using the default step size of 1 unit in the physical frame of the DWI image.
SetTotalTracts	Total Sampled Tracts: A positive integer that sets the total number tracts to sample from the seed voxel.
SetMaxLikelihoodCachSize	Maximum Likelihood Cache Size(MB) A positive integer that sets the maximum size of the Likelihood Cache in megabytes.
SetSeedIndex	Seed Voxel Index: The discrete index of the seed voxel, in the (IJK) reference frame of the image to start tractography.

Table 4.1: ITK Stochastic Tractography Filter Required Inputs and Parameters

```
ptfilterPtr->SetMaxLikelihoodCacheSize( maxlikelihoodcachesize );
ptfilterPtr->SetSeedIndex( seedindex );
```

The filter can then be run by calling the Update method.

```
ptfilterPtr->Update();
```

For the specified seed voxel, the filter outputs a connectivity map and a container holding all of the sampled tracts used to generate the connectivity map. The container of sampled tracts can be further processed outside of the stochastic tractography filter to obtain various statistic on the sampled tracts. Additional seed voxels can be included in the seed region by changing the seed voxel index and rerunning the filter. The statistics for a multi-voxel seed region can be analyzed by accumulating statistics for all seed voxels within the seed region. These outputs can be accessed by calling the `GetOutput` and `GetOutputTractContainer` methods after calling the `Update` method. The code below continues the example above and demonstrates how to obtain the filter's outputs.

```
PTFilterType::TractContainerType::Pointer tractcontainer =
  ptfilterPtr->GetOutputTractContainer();
CImageType::Pointer cmap = ptfilterPtr->GetOutput();
```

4.3 Command Line Module Interface

The command line module interface provides an easy to use method of performing common tasks which use the ITK stochastic tractography filter. The command line module takes as input a DWI volume, a white matter probability map and a label map to produce a connectivity probability map and fractional anisotropy and length statistics for a selected seed region in the label map. Currently the command line module is designed to work only with NRRD formatted volumes due to its support of the diffusion measurement frame, but future revisions of the software will extend support to other formats.

The command line module is named `StochasticTractographyFilter`. Calling the executable with the `--help` flag will list all available inputs and options as well as a short description of each item (Appendix B). This section will demonstrate two typical usages of the command line module interface.

Given a DWI volume, an associated white matter probability map and a label map, the command line module can be used to generate an image that provides the probability of connectivity from an ROI in the label map to all other voxels in the DWI. The label map is an integer valued image that segments voxels into different classes or labels.

Let `case24` be the name of the subject we are interested in analyzing. The directory `case24` contains all relevant files for that subject. It will also hold the output files generated by the command line module. Before executing the command line module interface, a possible list of files in the `case24` directory may include:

```
case24_DWI.nhdr (DWI NRRD header)
case24_DWI.raw (DWI NRRD data)
case24_whitematterPB.nhdr (White Matter Probability Map NRRD header)
case24_whitematterPB.raw (White Matter Probability Map NRRD data)
case24_labelmap.nhdr (Label Map NRRD data)
case24_labelmap.raw (Label Map NRRD data)
```

Assuming that the starting ROI is labeled 15 inside the labelmap, the stochastic tractography filter can be run by executing the command below within the `case24` directory: To run the command line module, execute the command:

```
StochasticTractographyFilter -c 6500 -m 500 -t 200 -e 15 -l 15
-r -o case24_RUN0 case24_DWI.nhdr case24_whitematterPB.nhdr
case24_labelmap.nhdr
```

After the command completes, the `case24` directory will contain the following additional files:

```
case24_RUN0_CMAP.nhdr (Connectivity Map NRRD header)
```

```
case24_RUN0_CMAP.raw (Connectivity Map NRRD data)
case24_RUN0_TENSOR.nhdr (Tensor image NRRD header)
case24_RUN0_TENSOR.raw (Tensor image NRRD data)
case24_RUN0_COND.nhdr (Conditioned Connectivity Map NRRD header)
case24_RUN0_COND.raw (Conditioned Connectivity Map NRRD data)
case24_RUN0_CONDFAValues.txt (Conditioned Tract-Averaged FA values)
case24_RUN0_CONDLENGTHValues.txt (Conditioned Tract Length values)
```

The conditioned connectivity map is identical to the normal connectivity map when the start label and end labels are the same. However, if the label map contains ROIs designated by two labels, the conditioned connectivity map will be generated using only fibers which start in the start ROI and also pass through the second ROI. Assuming the second ROI is labeled 2 in the labelmap, the following command will isolate tracts which start in the start ROI and pass through the end ROI:

```
StochasticTractographyFilter -c 6500 -m 500 -t 200 -e 2 -l 15
-r -o case24_RUN0 case24_DWI.nhdr case24_whitematterPB.nhdr
case24_labelmap.nhdr
```

Now the conditioned connectivity maps and statistics are generated using only tracts which fulfill the condition of passing through both ROIs. This feature allows us to analyze the particular bundle of tracts which connect two regions.

4.4 3D Slicer Interface

To encourage the algorithm's adoption in clinical studies, we created an interactive GUI module (Figure 4-3) for the 3D Slicer medical image visualization program was created which interfaces with the ITK stochastic tractography filter.

The module was implemented using the command line module interface provided by the 3D Slicer environment. This interface greatly eased the adaption of the command line interface into a graphical interface that could be included with 3D Slicer.

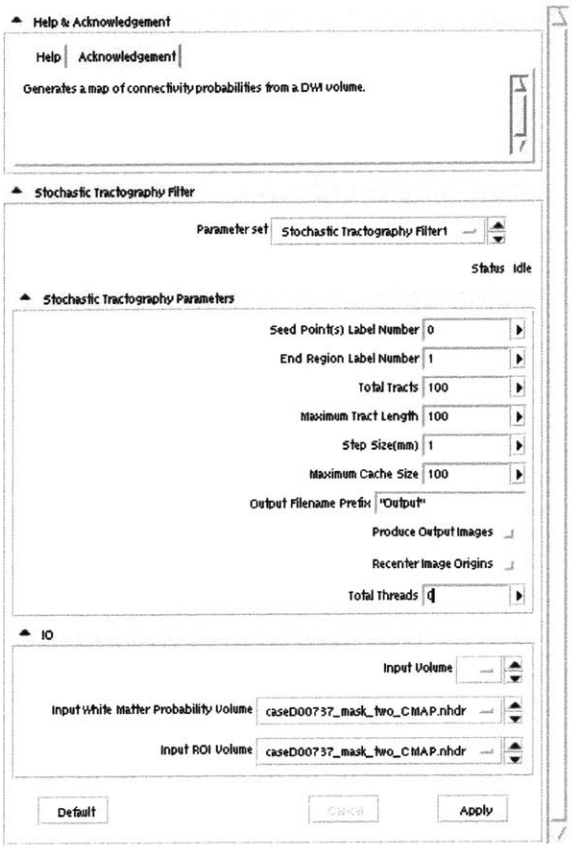

Figure 4-3: Stochastic Tractography GUI module within 3D Slicer.

The command line interface and the graphical interfaces are both completely described using an XML file. This XML file description is then parsed by a program provided by 3D Slicer which generates code that can be included with the command line interface to create what 3D Slicer refers to as a command line module. Command line modules can be run independently of 3D Slicer but can also be incorporated in to the 3D Slicer graphical interface. This enables the stochastic tractography system to function as an easy to use extension in the 3D Slicer program as well as a stand alone program suitable for processing a large numbers of data sets non-interactively. Appendix A includes a detailed description of the options for the command line module.

Chapter 5

Analysis of Right Internal Capsule Fibers

This chapter demonstrates the analysis of fibers originating from the right internal capsule in a single subject using the stochastic tractography system. We also demonstrate that by using a second ROI placed in the frontal lobe, we can restrict our analysis to tracts which start in the right internal capsule and progress towards the frontal lobe. Each analysis is performed with and without a white matter map to demonstrate differences in the results under these two conditions. Without the white matter map, tracts are allowed to pass through regions of gray matter, which may not have fiber bundles. Using the white matter map constrains the tracts to pass through only white matter known to have fiber bundles. Finally results obtained using stochastic tractography results are compared with those obtained under streamlining tractography. The DWI data set was obtained using 6 gradient directions and one B0 image obtained in the absence of diffusion weighted gradients. The voxels occupy 0.86mm x 0.86mm x 5mm sized cells. The right internal capsule was manually segmented using the fractional anisotropy image as a reference[1]. The right internal capsule segmentation is considered the first region of interest (ROI). A second region of interest(ROI) is placed anterior or towards the front of the brain, in the frontal lobe. Figure 5-1 displays the ROIs superimposed on the non-diffusion weighted b0

[1]ROIs created by Gudrun Rosenberger

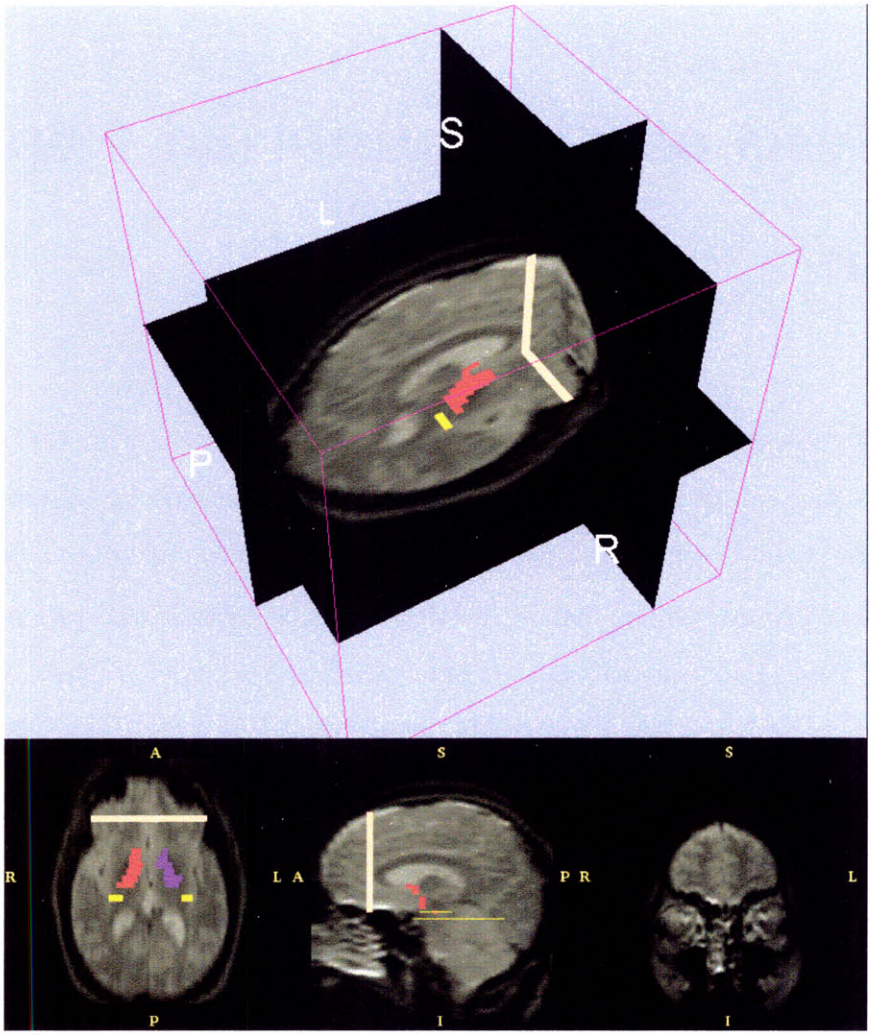

Figure 5-1: The non-diffusion weighted b0 image with superimposed right internal capsule and frontal lobe ROIs.

image of the DTI set.

In the results below, tractography was started in the right internal capsule ROI. The stochastic tractography system was initialized to sample 100 tracts from every voxel in the internal capsule. The actual number of samples collected may actually be less due to the use of a white matter map, which may exclude portions of the internal capsule ROI, or the rejection tracts which do not pass through a second ROI. Without using the white matter map, the tract was terminated when it left the brain or when it reached a maximum length of 500 mm. A whole brain mask was generated by running the FSL BET program [10] on the B0 image. The brain measures about 185 mm in diameter. Thus a 500 mm maximum tract length should be long to enough to generate all anatomically plausible tracts. When using a white matter map, tracts can only pass through regions of white matter and are terminated when they leave white matter. As a result, seed points in the gray matter cannot be used to initiate tractography. The white matter map was generated by running the FSL FAST program on the B0 image [23].

5.1 Single ROI

In this analysis all possible tracts originating from the right internal capsule ROI were sampled and included in the output.

Figure 5-2 presents connectivity maps generated using the stochastic tractography system. The color of each voxel indicates the number of tracts which pass through that voxel. Since seeding was initiated in the internal capsule, it appears highly connected to itself in the connectivity map. Notice the strong connectivity of some voxels in the frontal lobe using stochastic tractography with and without the white matter map. Without the white matter map 5-2(a) connections are dispersed throughout the brain. With the white matter map, the resulting spatial distribution of the fibers is more concentrated because false tracts are not generated in gray matter. Additionally, the number of sampled tracts when using the white matter map is reduced because the right internal capsule ROI may include some gray matter which cannot produce any

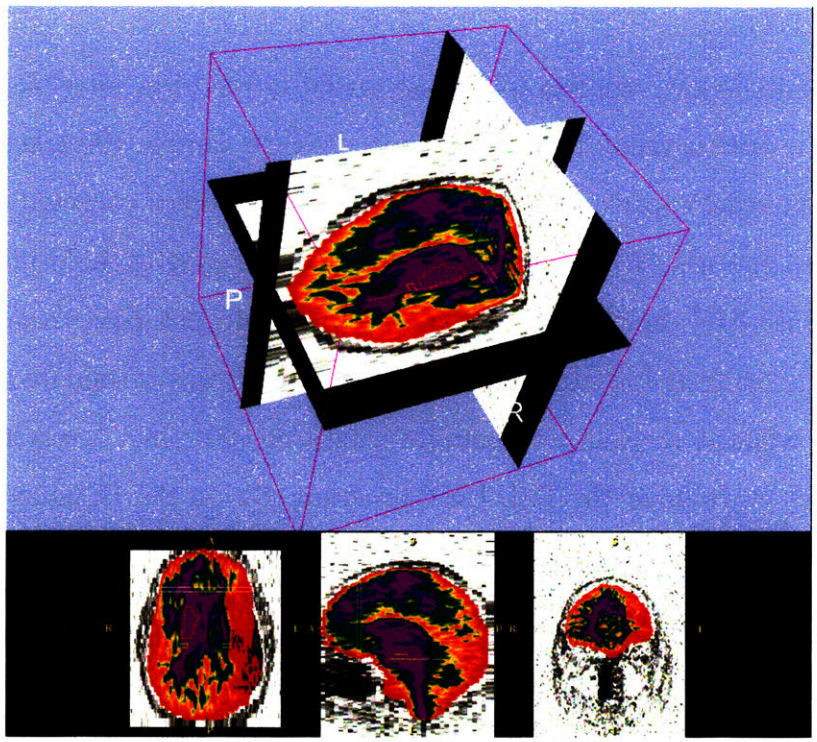

(a) Connectivity map generated without white matter map.

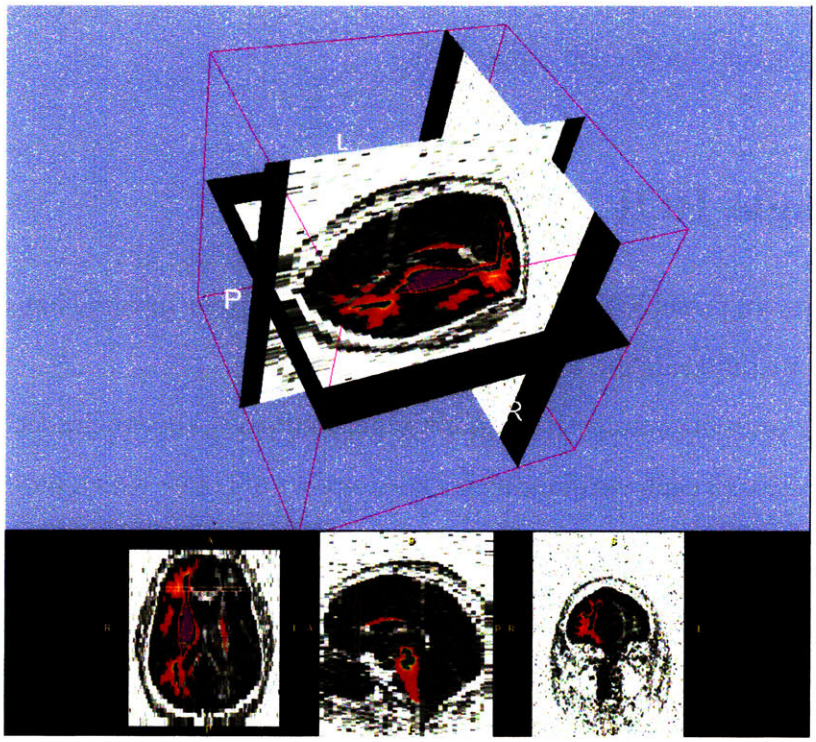

(b) Connectivity map generated with white matter map.

Figure 5-2: Connectivity maps generated using stochastic tractography overlaid on a fractional anisotropy image of the data. The seed region is the right internal capsule. The colors indicate the number of tracts originating from the seed region which pass through that voxel. Highly connected regions are purple while weaker connections are in red and yellow.

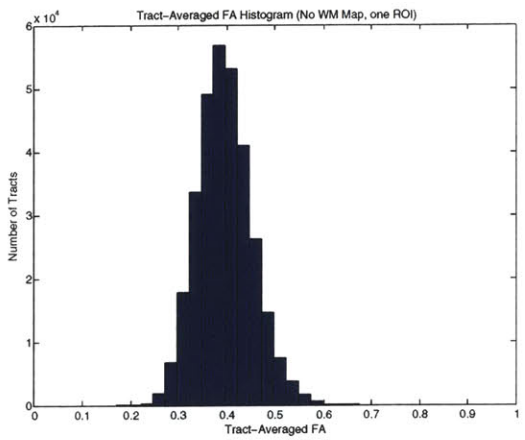

(a) Distribution without white matter map.

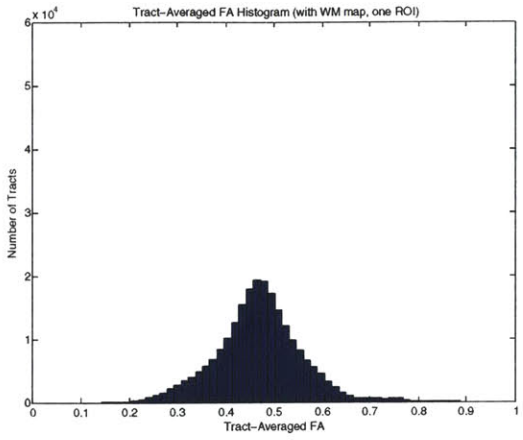

(b) Distribution with white matter map.

Figure 5-3: Histogram showing distribution of tract-averaged fractional anisotropy for tracts which originate in the right internal capsule.

tract samples.

We can also study statistics on individual sampled tracts. The distribution of tract-averaged fractional anisotropy is graphed in figure 5-3. Notice that using the white matter map predictably increases the mean of the distribution (Figure 5-3(a)), since the sampled tracts no longer pass through gray matter which has low anisotropy. Additionally, the number of sampled tracts also decreases when using the white matter map because some of the voxels in the right internal capsule ROI were identified as gray matter.

Figure 5-4 plots the distribution of lengths on the sampled tracts. Without the white matter map many fibers reach the arbitrary maximum tract limit of 500 (Figure 5-4(a), providing little information about the actual distribution of tract lengths. With the white matter posterior probability map, few sampled tracts reach 500mm and the distribution of tract lengths may be more representative of the true distribution.

5.2 Two ROIs

In addition to sampling all possible fibers from a seed region, the stochastic tractography system can optionally reject all sampled tracts which do not pass through a

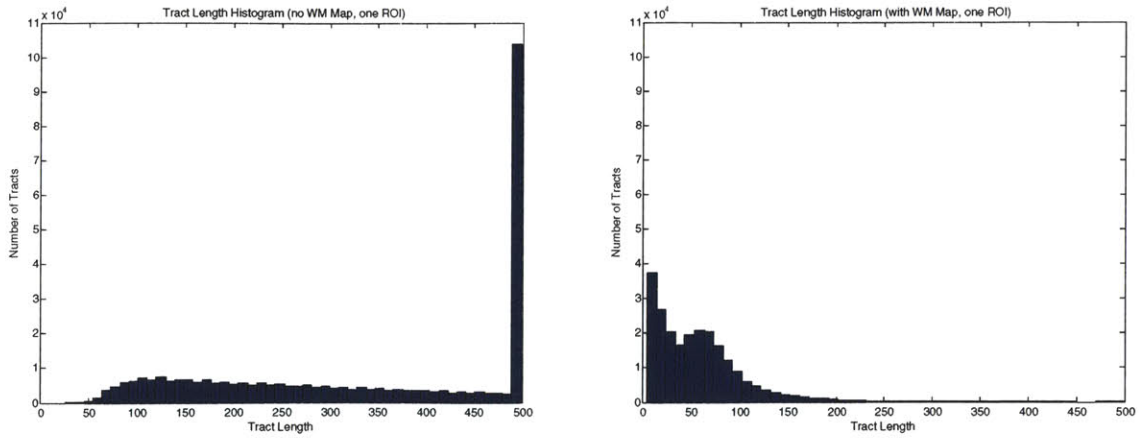

(a) Distribution without white matter map.

(b) Distribution with white matter map.

Figure 5-4: Histogram showing distribution of fiber lengths for sampled frontal lobe tracts.

second ROI. This method isolates fiber bundles which connect two ROIs.

The connectivity maps in Figure 5-5 show the probability that a voxel is connected to the right internal capsule by a fiber originating in the right internal capsule which passes through the second ROI located in the frontal lobe. Unsurprisingly, regions in the frontal lobe are much more likely to be connected via these fibers than anywhere else in the brain.

Although 100 tract samples were attempted by the algorithm, only a fraction pass through the second ROI. Thus the histograms in figures 5-6 and 5-7 contain fewer total tracts than those in figures 5-3 and 5-4. Notice that using the white matter map again increases the mean of the tract-averaged fractional anisotropy distribution (Figure 5-6(b)) by preventing tracts from passing through low anisotropy gray matter.

Figure 5-7 demonstrates that using the white matter map provides more meaningful distributions of length than tracking without using one.

5.3 Comparison with streamlining tractography

In this section, we compare the results of streamlining tractography and stochastic tractography from the same data using the same ROIs. The streamlining tractography results are generated using the streamline tractography method in 3D Slicer. The

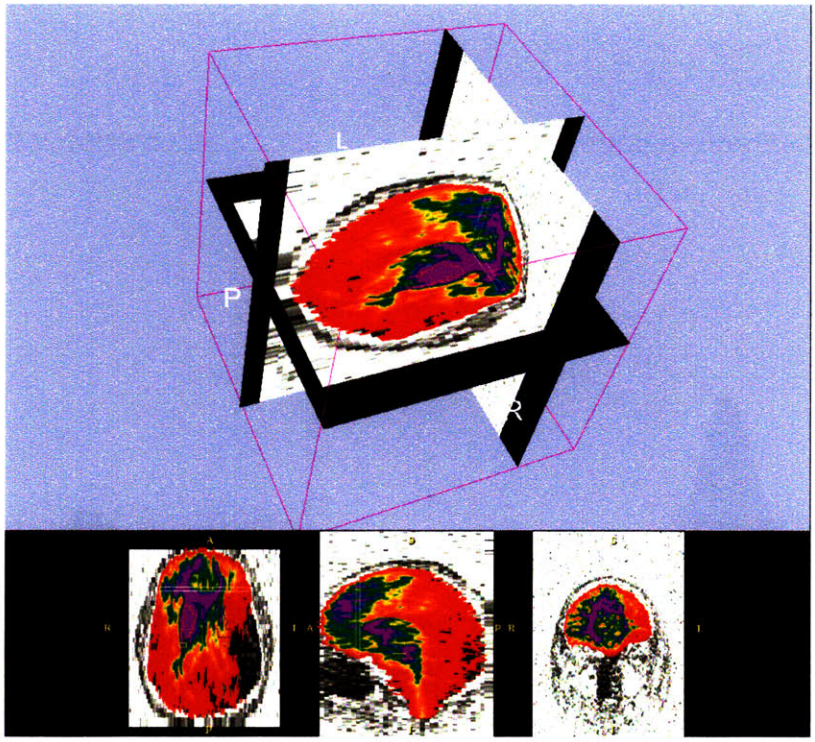

(a) Connectivity map generated without white matter map.

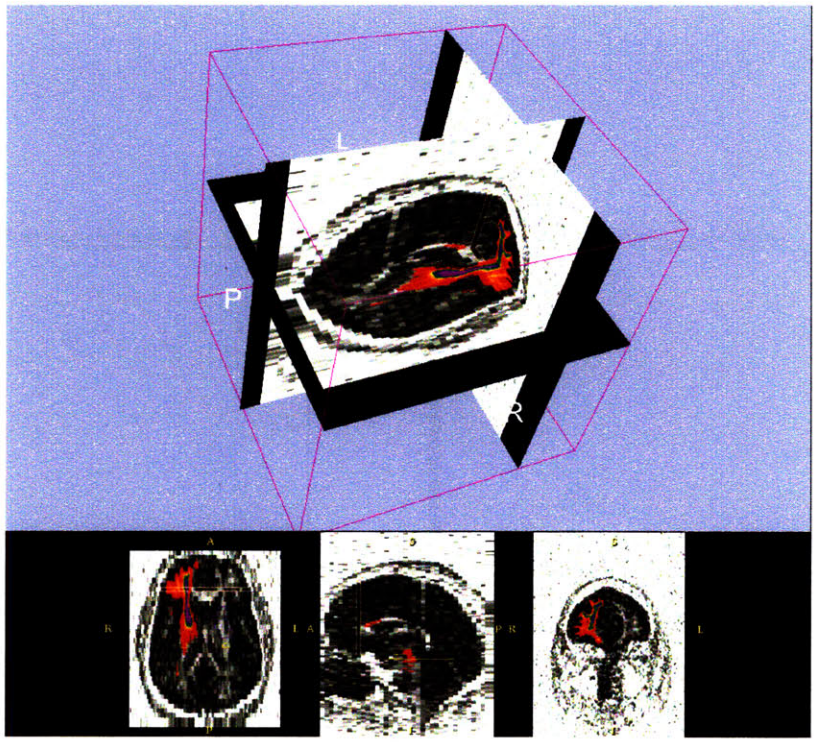

(b) Connectivity map generated with white matter map.

Figure 5-5: Connectivity map overlaid on a fractional anisotropy image showing the probability that a voxel is connected to the internal capsule by a fiber which passes through a second ROI in the frontal lobe.

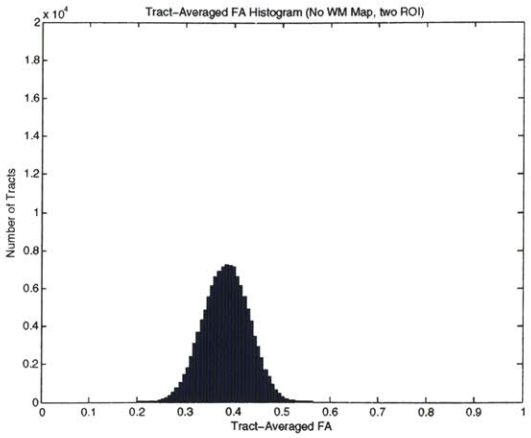

(a) Distribution without white matter map.

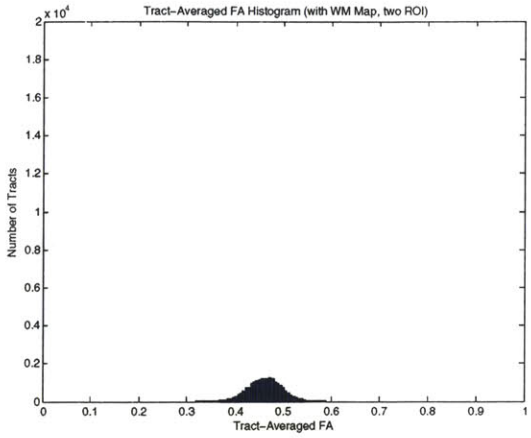

(b) Distribution with white matter map.

Figure 5-6: A histogram of tract-averaged fractional anisotropy for fibers which originate in the right internal capsule and pass through an ROI in the frontal lobe.

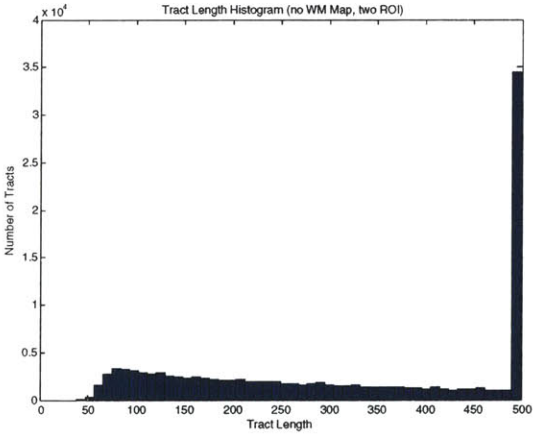

(a) Distribution without white matter map.

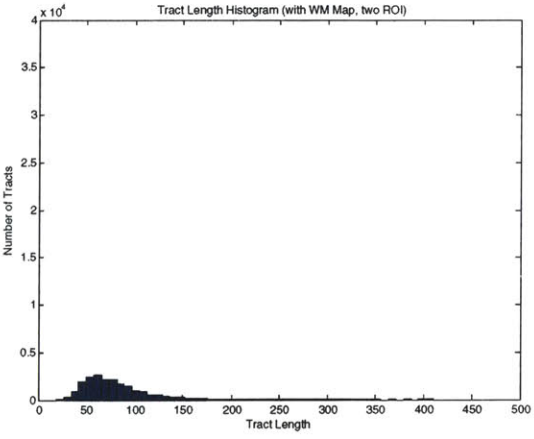

(b) Distribution with white matter map.

Figure 5-7: A histogram of lengths for sampled fibers which start in the right internal capsule and pass through the ROI in the frontal lobe.

streamline method used every voxel inside the segmented internal capsule as a seed region. The generated streamline tracts were only accepted if they passed through the second ROI in the frontal lobe. Tracking was terminated in the streamline method when the current voxel's anisotropy fell below a minimum threshold. The stochastic tractography results were those reported in the previous section and depicted in figures 5-6 and 5-7.

Figures 5-8 and 5-9 visually compare the results of streamlining and stochastic tractography results using the same input data and ROIs. Figure 5-9 overlays a volume rendering of the connectivity map generated using stochastic tractography on the tracts generated using the streamlining method. In this image the gray/black cloud is a 3D rendering of the connectivity map. Although it is difficult to gauge the degree of connectivity in the volume rendering, it is clear that there exist regions which, according to stochastic tractography, have nonzero probability of connectivity but do not have streamline tracts passing through them. Additionally, notice that in the region of the most inferior, or downward, streamline tracts, the stochastic tractography reports relatively weak connectivity. The streamline method generates tracts in this improbable region because the anisotropy in this area is above the minimum threshold. However since the stochastic tractography method takes into account the uncertainty in fiber direction, it determines that these tracts are much less likely to occur than a tract which is more superior, or upwards.

Figure 5-10 compares tract-average FA distributions of the same tracts of interest under stochastic and streamlining tractography. The histograms are both approximately normal with some left skew under streamlining tractography. The distribution under stochastic tractography is very smooth because the sample size is much larger than under streamlining tractography. In stochastic tractography many possible tracts can be sampled from a single seed voxel while only one tract per seed voxel can be generated under streamlining tractography resulting in a maximum of 1,372 tracts. Additionally, the mean of the distribution under stochastic tractography is higher than under streamlining tractography. Since FA is related to uncertainty, stochastic tractography will generate more tracts which pass though regions of high

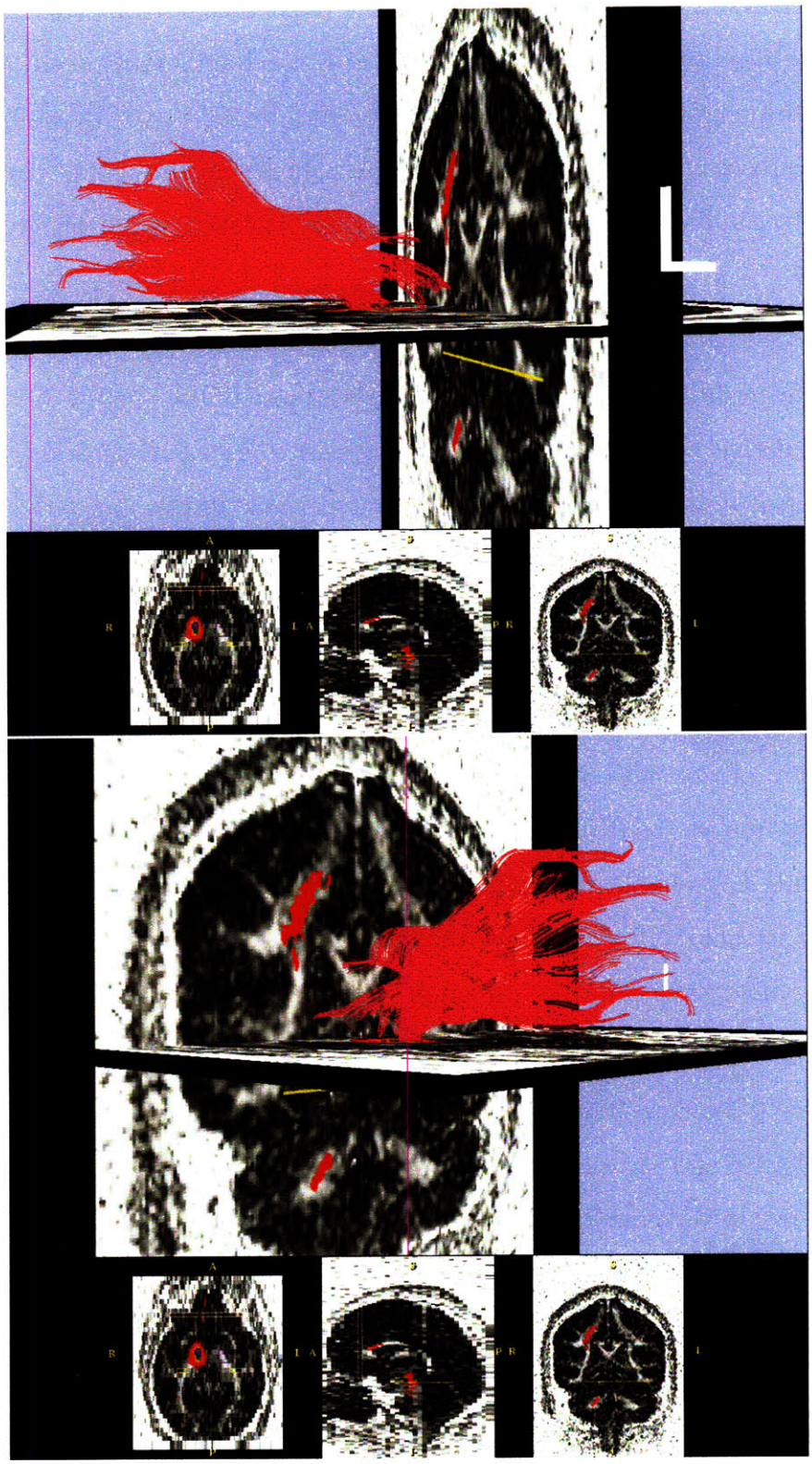

Figure 5-8: A rendering of tracts generated using streamlining tractography for tracts which originate in the right internal capsule and pass through a second ROI in the frontal lobe.

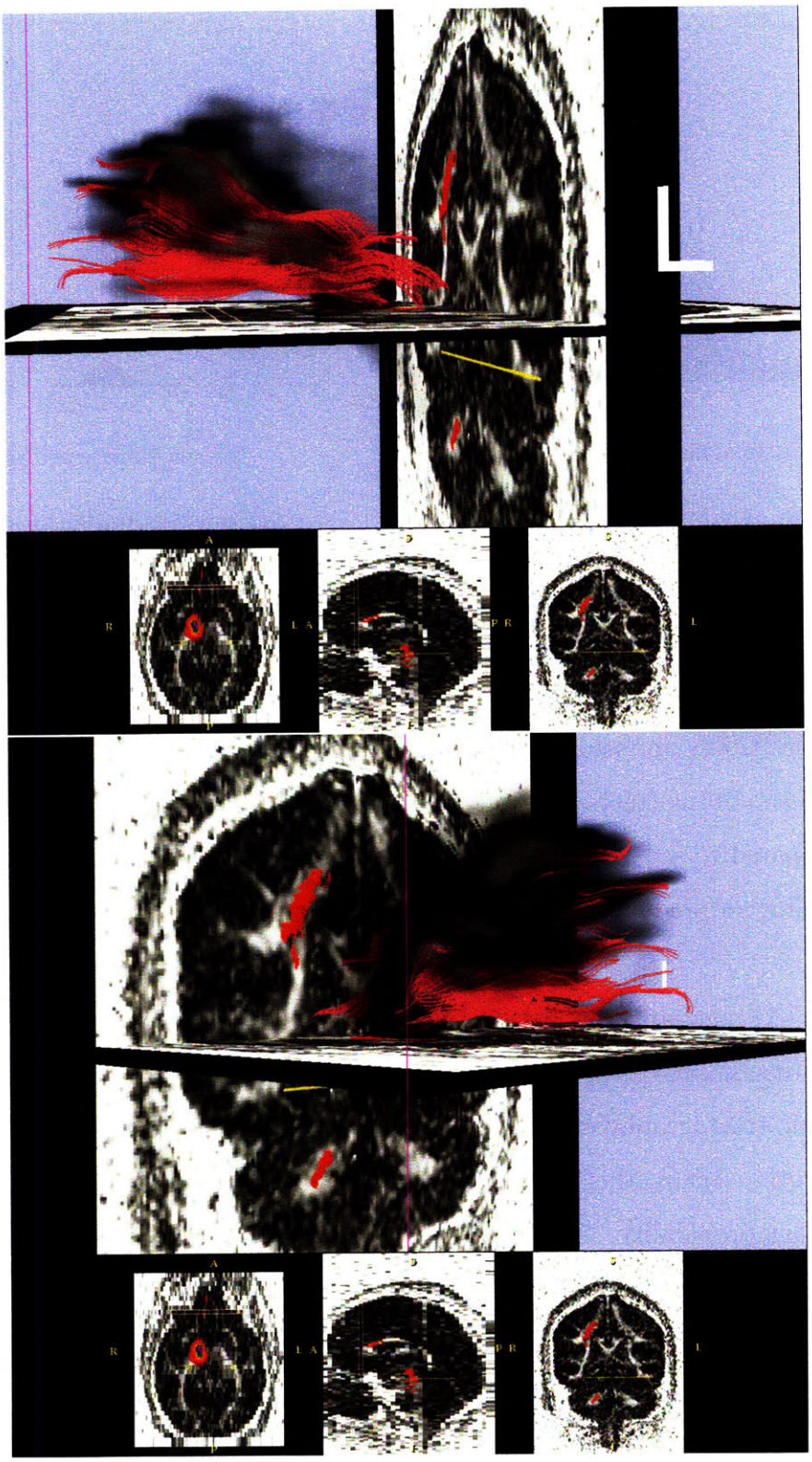

Figure 5-9: A volumetrically rendered connectivity map generated using stochastic tractography overlaid on tracts generated using streamlining tractography. The results are generated using identical input data and ROIs.

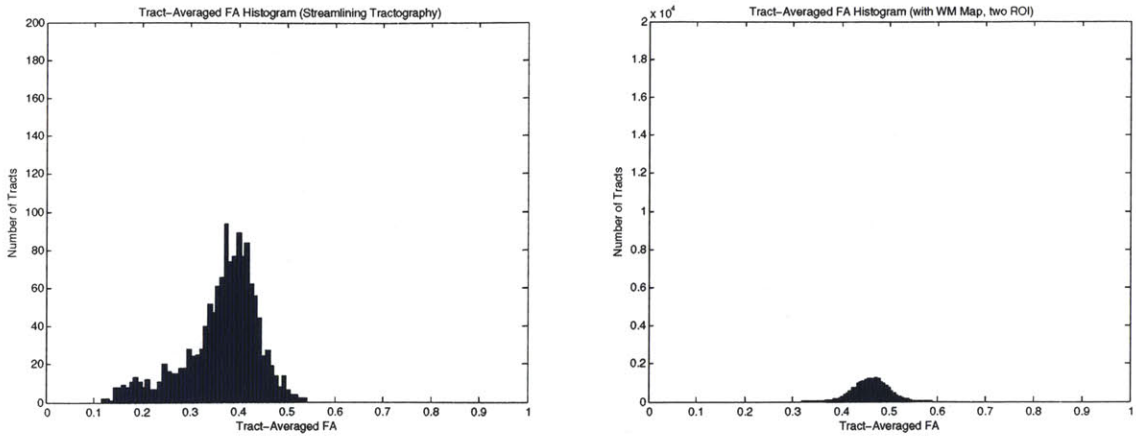

(a) streamlining tractography

(b) stochastic tractography

Figure 5-10: A comparison of tract-averaged FA distributions under stochastic and streamlining tractography. Only tracts which originate from the right internal capsule and pass through a second ROI in the frontal lobe are included. Notice the y-axis for the streamlining tractography histogram has been scaled up by a factor of 100 due to the relatively few number of tracts generated using streamlining.

FA. As more tracts are sample they will tend to concentrate in regions of high FA. Thus the mean of the tract-average FA distribution is increased in stochastic tractography compared to streamlining tractography. This affect may not be as prominent when tracking in predominantly isotropic regions as this concentrating effect is not present.

Figure 5-11 compares the distribution of tract lengths under stochastic tractography and streamlining cases. While the distributions look similar, increased sampling in stochastic tractography eliminates the shorter tracts in favor of tracts around 50 mm in length. Again, this is due to stochastic tractography's ability to take into account tract probability. Also, the similarity in the distributions further suggests that the stochastic tractography tract length distribution is informative only when a white matter map is used.

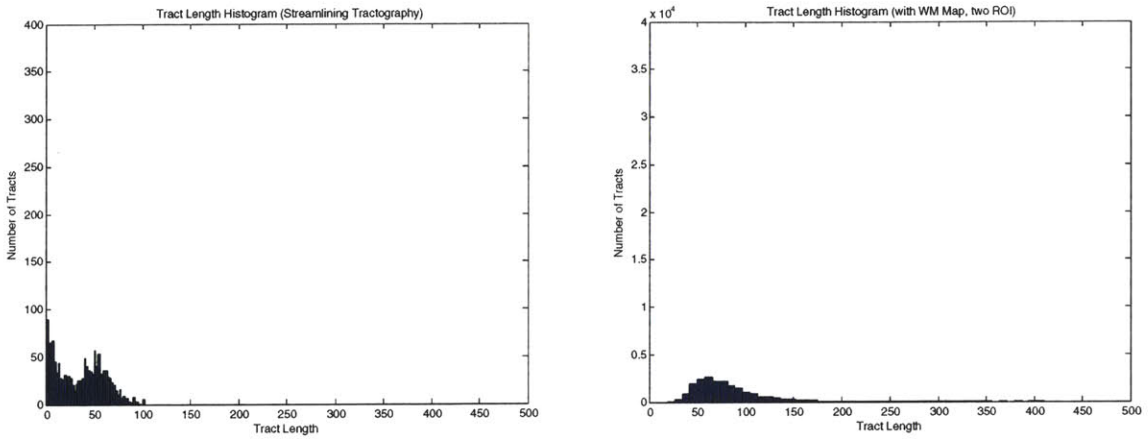

(a) streamlining tractography

(b) stochastic tractography

Figure 5-11: A comparison of tract length distributions distributions under stochastic and streamlining tractography. Only tracts which originate from the right internal capsule and pass through a second ROI in the frontal lobe are included. Notice the y-axis for the streamlining tractography histogram has been scaled up by a factor of 100 due to the relatively few number of tracts generated using streamlining.

Chapter 6

Discussion and conclusions

In this project we implemented a system for analyzing white matter architecture from DTI images. The multithreaded implementation of the system allows parallel sampling of fiber tracts, reducing computation time on multi-processor systems. To facilitate the algorithm's use in clinical studies, an easy to use graphical interface was created for the 3D Slicer visualization program. Furthermore, we demonstrate the system's characteristics through an analysis of fibers originating from the right internal capsule. In this section, we will discuss some possible extensions to the system and present an outline for a potential clinical study which investigates frontal lobe fibers in schizophrenia using the stochastic tractography system developed in this thesis.

6.1 Potential Extensions

The design of the stochastic tractography system is not tightly coupled and thus allows the tensor parameter estimation engine to be replaced. In the presented work, the stochastic tractography system estimates the log tensor model parameters through weighted least squares estimation. More robust techniques of tensor model parameter estimation have been proposed by Koay et al. [13]. We can refine the fiber orientation likelihood function in our system using these improved tensor model parameter estimates. Ideally, the DTI image and estimated B0 image should be calculated before

the stochastic tractography system is run. The stochastic tractography system can take this DTI image and B0 image as input in lieu of the DWI image. This approach allows the researcher to use any arbitrary tensor model parameter estimation engine and additionally makes stochastic tractography faster as the tensor parameters would not need to be calculated at run time. The modifications required to implement this feature is relatively minor, but the user interface must be designed thoughtfully to minimize the added complexity of these new options.

Although DTI images can be illumination of changes in anisotropy, DTI data alone is insufficient to determine the causes of changes in anisotropy. Reduced anisotropy can stem from a decoherence in a fiber bundle's structure, losses in myelin, and other abnormalities. Kubicki et al. [14] attempted to clarify the cause of changes in anisotropy by comparing information about nerve fiber integrity that are inferred from DTI and MTR. MTR is an MR scanning technique that provides information regarding the distribution of myelin in the brain. Anisotropy changes that are detectable by both MTR and DTI suggest alterations to the myelin. Changes that are detectable only by DTI suggest decoherence in the fiber's structure. The algorithm can be further extended by incorporating information from MTR measurements [14] into the Bayesian framework.

6.2 Study of frontal lobe fibers in schizophrenia

We conclude by describing a potential group study of frontal lobe fiber differences in Schizophrenia using the stochastic tractography system. This group study is an extension of the single subject analysis of frontal lobe fibers presented in the previous chapter. The study also provides an opportunity to compare findings using stochastic tractography with those previously obtained from streamlining tractography on identical data sets.

6.2.1 Background

Schizophrenia is neurological disorder whose characteristic symptoms include hallucinations and disorganized thinking. Scientists have suggested that the pathology of schizophrenia may involve anatomical abnormalities including abnormal white matter architecture. Clinical DTI studies have demonstrated differences in diffusion anisotropy within fiber tracts in Schizophrenia patients compared with healthy patients [15],[14].

White matter architecture abnormalities related to schizophrenia may include a reduction in the integrity or amount of the myelin, increased disorganization of fibers which constitute certain fiber bundles, or a reduction in the number of fibers comprising a fiber bundle. Myelin, the fatty insulator which surrounds the axons, is believed to be a major barrier to water diffusion. Degradation of the myelin permits increased diffusion perpendicular to the orientation of the fibers which can be observed as reduced anisotropy in DTI data. Also the orientation of axon fibers which comprise a fiber bundle may be less directionally coherent in Schizophrenia. Since many fibers pass through a single voxel and the resultant diffusion distribution is an average of diffusion of all water molecules in that voxel, a voxel containing fibers which are less coherent may have reduced anisotropy. The fiber bundles may also be less dense in Schizophrenia. A reduction in axon density would result in reduced anisotropy since water molecules are more free to diffuse perpendicularly to the tracts. These structural deficiencies result in poorer conduction of action potentials between different regions of the brain leading to reduced functional connectivity. The fibers that connect the thalamus and the frontal lobe are believed to be involved in memory formation. These fibers are depicted in figure 6-1. Since Schizophrenia patients have difficulty forming and organizing memory, deficiencies in these fibers may explain these symptoms. Additionally these fibers present an interesting tractography problem because there are many other fibers which cross this set of fibers on their way to the frontal cortex. In these regions of crossing, the diffusion is averaged with the crossing fibers resulting in a diffusion profile with reduced anisotropy. This is precisely the situ-

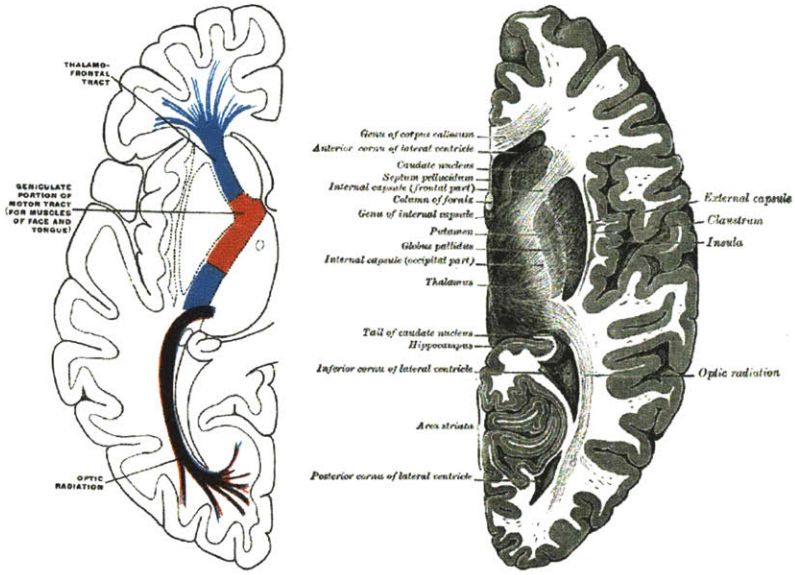

Figure 6-1: The Thalamus, the Internal Capsule and fibers. We wish to characterize the fibers which originate in the thalamus, pass through the internal capsule and end in the frontal cortex. This image is from Gray's Anatomy.

ation that stochastic tractography can be useful since streamlining methods would terminate in regions of low anisotropy possibly never reaching the frontal cortex. In this future study, we will analyze these fibers in schizophrenia and control groups to determine whether schizophrenia patients exhibit lower tract-averaged fractional anisotropy than the control group. Additionally, we will compare results obtained using stochastic tractography with previous streamline tractography results.

6.2.2 Method

We will first obtain DWI data sets for as many schizophrenia and control subjects as possible. Each DWI data set will consist of at least six gradient weighted images and one baseline image as this is the minimum required for the stochastic tractography system. Additionally we will create a white matter map for each subject either by a segmentation of an additional anatomical image obtained during the DWI acquisition or through the segmentation of the B0 image. Label maps for the right and left internal capsules for each subject are created through expert manual segmentation. An additional ROI is placed in the frontal lobe to isolate fibers which originate in the

internal capsules and proceed towards the frontal lobe.

The stochastic tractography system will then used to generate tract length and tract-averaged FA statistics for tracts which originate in the right internal capsule and pass through the frontal lobe ROI. The system will be run again for tracts which originate in the left internal capsule and pass through frontal lobe ROI. These analysis will be performed for all subjects. Tracts will be sampled until the mean of the length and tract-averaged FA distributions show a degree of stability with respect to the number of samples.

Assuming that the mean tract-averaged FA is normally distributed, a t-test can be used to determine whether the mean of the mean tract-averaged FA differs significantly between schizophrenia subjects and normal subjects. The same is performed for the distribution of tract lengths.

Finally, these results will be compared with the results of a streamline tractography based study on the same data set by Rosenberger[20]. This study found significant differences in the mean of the mean tract-averaged FA between schizophrenia and control groups.

6.3 Summary

The field of neuroscience has made great advances in recent years. Further understanding of how the brain functions and the diseases which affect it will depend on our ability to study white matter architecture. In-vivo observation techniques such as Diffusion Tensor MRI play a crucial role in the study of white matter architecture. As observation methods become more sophisticated, our tools for inference must also be sufficiently sophisticated to extract the valuable information hidden in these observations. The stochastic tractography system we have presented in this thesis provide neuroscientists with an efficient and easy to use tool to characterize white matter architecture.

Appendix A

Command Line Module Interface

Below is the automatically generated output of the command line module when running the StochasticTractographyFilter program with the `--help` option.

```
USAGE:

   StochasticTractographyFilter  [--processinformationaddress
                                 <std::string>] [--xml] [--echo] [-j <int>]
                                 [-r] [-i] [-o <std::string>] [-c <int>]
                                 [-s <int>] [-m <int>] [-t <int>] [-e
                                 <int>] [-l <int>] [--] [--version] [-h]
                                 <std::string> <std::string> <std::string>


Where:

   --processinformationaddress <std::string>
     Address of a structure to store process information (progress, abort,
     etc.). (default: 0)

   --xml
```

```
  Produce xml description of command line arguments (default: 0)

--echo
  Echo the command line arguments (default: 0)

-j <int>,  --totalthreads <int>
  Total number of threads to use.  Default value of zero sets number of
  threads to number of CPUs (default: 0)

-r,  --recenteroriginswitch
  Ignore the origins of the ROI and WM mask and set it to be the same as
  the DWI image origin (default: 0)

-i,  --outputimageswitch
  Output Tensor, FA maps and Connectivity Maps (default: 0)

-o <std::string>,  --outputprefix <std::string>
  Prefix for the output files (default: "Output")

-c <int>,  --maxlikelihoodcachesize <int>
  Maximum Size of Likelihood Cache (default: 100)

-s <int>,  --stepsize <int>
  The length of each segment of the tract in mm (default: 1)

-m <int>,  --maxtractlength <int>
  Maximum Length of Sample Tract (default: 100)

-t <int>,  --totaltracts <int>
  Number of Sample Tracts (default: 100)
```

-e <int>, --endlabelnumber <int>

Label Number to use as end region (default: 1)

-l <int>, --labelnumber <int>

Label Number to use as seed points (default: 0)

--, --ignore_rest

Ignores the rest of the labeled arguments following this flag.

--version

Displays version information and exits.

-h, --help

Displays usage information and exits.

<std::string>

(required) Input DWI volume to be filtered

<std::string>

(required) Input Mask volume that provides the probability that the voxel is white matter

<std::string>

(required) Input ROI volume used to seed algorithm

Description: Generates a map of connectivity probabilities from a DWI volume.

Author(s): Tri Ngo

Bibliography

[1] C. Andrieu, N. de Freitas, A. Doucet, and M. Jordan. An introduction to mcmc for machine learning, 2003.

[2] PJ Basser and S. Pajevic. In vivo fiber tractography using dt-mri data. *Magn Reson Med*, 44:625–632, 2000.

[3] T.E.J Behrens, M.W. Woolrich, M. Jenkinson, H. Johansen-Berg, R. G. Nunes, S. Clare, P.M. Matthews, J.M Brady, and S.M. Smith. Characterization and propagation of uncertainty in diffusion-weighted mr imaging. *Magnetic Resonance in Medicine*, 50:1077–1088, 2003.

[4] M. Björnemo, A. Brun, R. Kikinis, and C.-F. Westin. Regularized stochastic white matter tractography using diffusion tensor MRI. In *Fifth International Conference on Medical Image Computing and Computer-Assisted Intervention (MICCAI'02)*, pages 435–442, Tokyo, Japan, 2002.

[5] Brigham and Women's Hospital. 3d slicer medical visualization and processing environment for research. *http://www.slicer.org/*.

[6] Ching-Po, Wen-Yih Issac Tseng, Hui-Cheng Cheng, and Jyh-Horng Chen. Validation of diffusion tensor magnetic resonance axonal fiber imaging with registered manganese-enhanced optic tracts. *Neuroimage*, 14, 2001.

[7] Insight Software Consortium. National library of medicine insight segmentation and registration toolkit(itk). *http://www.itk.org/*.

[8] O. Friman and C.-F. Westin. Uncertainty in fiber tractography. In *Eighth International Conference on Medical Image Computing and Computer-Assisted Intervention (MICCAI'05)*, Lecture Notes in Computer Science 3749, pages 107–114, Palm Springs, CA, USA, October 2005.

[9] Ola Friman, Gunnar Farneback, and Carl-Fredrik Westin. A Bayesian approach for stochastic white matter tractography. *TMI*, 25(8):965–978, 2006.

[10] M. Jenkinson, M. Pechaud, and S. Smith. Bet2: Mr-based estimation of brain, skull and scalp surfaces. *Eleventh Annual Meeting of the Organization for Human Brain Mapping*, 2005.

[11] Derek K. Jones and Carlo Pierpaoli. Confidence mapping in diffusion tensor magnetic resonance imaging tractography using a bootstrap approach. *Magnetic Resonance in Medicine*, (5):1143–1149, 2005.

[12] Gordon Kindlmann and Carl-Fredrik Westin. Diffusion tensor visualization with glyph packing. *IEEE Transactions on Visualization and Computer Graphics (Proceedings Visualization / Information Visualization 2006)*, 12(5):(to appear), September-October 2006.

[13] Cheng Guan Koay, Lin-Ching Chang, John D. Carew, Carlo Pierpaoli, and Peter J. Basser. A unifying theoretical and algorithmic framework for least squares methods of estimation in diffusion tensor imaging. *Journal of Magnetic Resonance*, 182:115–125, 2006.

[14] M. Kubicki, H.-J. Park, C.-F. Westin, P. Nestor, R. Mulkern, S. E. Maier, M. Niznikiewicz, E. Connor, J. Levitt, M. Frumin, R. Kikinis, F. A. Jolesz, R. McCarley, and M. E. Shenton. DTI and MTR abnormalities in schizophrenia: Analysis of white matter integrity. *Neuroimage*, 26:1109–1118, 2005.

[15] M. Kubicki, C.-F. Westin, S. E. Maier, H. Mamata, M. Frumin, H. Ernst-Hirshefeld, R. Kikinis, F. A Jolesz, R. W. McCarley, and M. E. Shenton. Cin-

gulate fasciculus integrity disruption in schizophrenia: A magnetic resonance diffusion tensor imaging study. *Biological Phychiatry*, 54:1171–1180, 2003.

[16] M. Kubicki, C.-F. Westin, R. McCarley, and M. E. Shenton. The application of dti to investigate white matter abnormalities in schizophrenia. *Ann NY Acad Sci*, 1064:134–148, 2005.

[17] M. Lazar and A. Alexander. Bootstrap white matter tractography (boot-trac). *NeuroImage*, 24:524–532, 2005.

[18] S. Mori, B. Crain, V.P. Chacko, and PCM van Zijl. Three dimensional tracking of axonal projections in the brain by magnetic resonance imaging. *Ann Neurol*, 45:265–269, 1999.

[19] Lauren O'Donnel. Cerebral white matter analysis using diffusion imaging.

[20] Gudrun Rosenberger. Group study of frontal lobe fibers in schizophrenia. *Unpublished*, 2007.

[21] Raymond Salvador, Alonso Pena, David K. Menon, T. Adrian, T. Adrian Carpenter, John D. Pickard, and Ed T. Bullmore. Formal characterization and extension of the linearized diffusion tensor model. *Human Brain Mapping*, 24:144–155, 2005.

[22] D.S. Tuch, M.R. Wiegell, T.G. Reese, J.W. Belliveau, and V.J. Weeden. Measuring cortico-cortical connectivity matrices with diffusion spectrum imaging. In *Proc. of the International Society for Magnetic Resonance Medicine*, page 502, Glasgow, Scotland, 2001.

[23] Y. Zhang, M. Brady, and S. Smith. Segmentation of brain mr images through a hidden markov random field model and the expectation maximization algorithm. *IEEE Trans. on Medical Imaging*, 54(1):45–57, 2001.